Synthesis and Conjugation of D-glycero-β-D-mannoheptose 1-monophosphate

Owere Okeny

Thesis submitted to the University of Ottawa
in partial Fulfillment of the requirements for the
Master of Science Chemistry

Department of Chemistry and Biomolecular Sciences
Faculty of Science
University of Ottawa

Abstract

Pathogen-associated molecular patterns (PAMPs) are molecular motifs of microbes that are not produced by the host. PAMPs are recognized by pattern recognition receptors that lead to the activation of a host immune response. As such, they are promising molecular scaffolds for use in immune modulating therapies; however, there are challenges associated with translating them to the clinic. D-glycero-β-D-mannoheptose 1-monophosphate (HMP) is an example of a PAMP with a carbohydrate scaffold that shows promise for use as an immune agonist. However, administering this sugar without chemical modifications requires cell membrane permeabilization due to its limited ability to enter cells. Finding a route to administer this PAMP without altering the cell membrane is a significant challenge and limits its testing in animal models and potential use as a drug. To address this, we proposed to conjugate D-glycero-β-D-mannoheptose 1-monophosphate to spherical nucleic acids, which are DNA-nanoparticle conjugates known to enter cells unaided. In this work, a large-scale synthesis of aminoethyl-D-glycero-β-D-mannoheptose 1-monophosphate was performed. The incorporation of an amine on this compound enabled its derivatization with an azide to form N_3-PEG_4-7-O-(amidoethyl)-D-glycero-β-D-manno-heptopyranose phosphate, which was conjugated to dibenzocyclooctyne (DBCO)-functionalized oligonucleotides synthesized by the Bujold group at McMaster University. These N_3-PEG_4-7-O-(amidoethyl)-D-glycero-β-D-manno-heptopyranose phosphate-functionalized oligonucleotides were then densely functionalized onto gold nanoparticles to form the desired spherical nucleic acids.

Acknowledgements

Thank you greatly to my three supervisors: Dr. Janelle Sauvageau, Dr. Katherine Bujold, and Dr. Chris Boddy. It is a privilege to learn from any one of you, and a luxury to have learned from all three of you. Thank you to Mimi Han and the Bujold group for their oligonucleotide synthesis and support. Dr. Janelle Sauvageau, and Parsa Jamshidi, thank you for all the patient guidance and support throughout the project. Thank you, Jacek Stupak and Kenneth Chan, for MS expertise you both provided. PAGE analysis was greatly supported by Denis Brochu, thank you for all the help you provided. Thank you to Dr. Sharon Bardon for the MALDI-TOF analytics instruction, guidance, and general willingness to help. I have been encouraged to strive to be my best by my committee Dr. Jeffery Keillor and Dr. Adam Shuhendler, thank you for taking time to review my work.

Contributions

Dr. Janelle Sauvageau and Dr. Katherine Bujold contributed their time and expertise in guiding the direction of this work. NMR guidance was provided by Dr. Janelle Sauvageau, Parsa Jamshidi, and Dean Williams. MS guidance was provided by Ken Chan. HPLC development and optimization was supported by Dean Williams. In this work all the oligonucleotides were synthesized by Dr. Katherine Bujold and Mimi Han. PAGE analysis was supported by Dr. Bujold, and Denis Brochu from the NRC. MALDI-TOF was performed by Ken Chan at the NRC. MALDI-TOF guidance was provided by Dr. Sharon Barden at the John L. Holmes Mass Spectrometry facility (University of Ottawa). SPAAC chemistry was performed by Dr. Bujold, in addition to characterization of molecule **2**. DNA characterization was supported by Dr. Katherine Bujold and Mimi Han.

Abbreviations

FmocCl = Fmoc Chloride

RT = Room Temperature

DCM = Dichloromethane

PMBCl = *p*-methoxy benzyl chloride

TFA = Trifluoroacetic Acid

DIBAL = Diisobutylaluminium hydride

Et_3N = Triethylamine

TEMED = Tetramethylethylenediamine

DBCO-Cy5-T20 = DBCO-Cyanine5-Thymine20

BMS = Borane dimethyl sulfide

DPPC = Diphenylphosphoryl chloride

TEAB = Triethylammonium Bicarbonate buffer

CHCA= α-Cyano-4-hydroxycinnamic acid

PAGE = Polyacrylamide gel electrophoresis

PAMP = Pathogen Associated Molecular Pattern

SR-A = Scavenger Receptor-A

SNA = Spherical Nucleic Acid(s)

ACN = Acetonitrile

S7P = sedoheptulose 7-phosphate

HBP = D-glycero-β-D-mannoheptose 1,7-bisphosphate

HMP-7 = D-glycero-D-manno-heptose 7-phosphate

HMP = D-glycero-β-D-mannoheptose 1-monophosphate

HMP-LINK = PEG4-7-O-(amidoethyl)-D-glycero-β-D-manno-heptopyranose phosphate

HMP-Cy5-T20 = T20-Cy5-PEG4-7-O-(amidoethyl)-D-glycero-β-D-manno-heptopyranose phosphate

HMP-Cy5-T13-7GUA = T13-7GUA- PEG4-7-O-(amidoethyl)-D-glycero-β-D-manno-heptopyranose phosphate

HPA = 3-hydroxypicolinic acid

DHAP = 2,6-dihydroxyacetophenone

APS = Ammonium Persulfate

NRC = National Research Council of Canada

T20 = Thymine20

ART = Antiretroviral Therapy

cART = combined Antiretroviral Therapy

AIDS = Acquired Immunodeficiency Syndrome

LRA = Latency Reversal Agent

Table of Contents

Table of Figures

Table of Schemes

Aims of this work

This study aims to improve the uptake of D-glycero-β-D-mannoheptose 1-monophosphate (HMP) in the HCT 116 cell line. This cell line was selected because it expresses the scavenger receptor-A and was used in prior studies with HMP. The first aim was to synthesize an HMP derivative with an azide group to enable its conjugation via click chemistry to oligonucleotides containing DBCO at the 5' end and a thiol at the 3' end (Figure *1*). The second aim was to conjugate the DNA-HMP conjugates onto gold nanoparticles to form SNAs. The third aim was to administer these SNAs (**1**) to HCT 116 cells then measure the IL-8 response using ELISA, and use confocal microscopy, as well as flow cytometry to assess if uptake has improved (Figure 2).

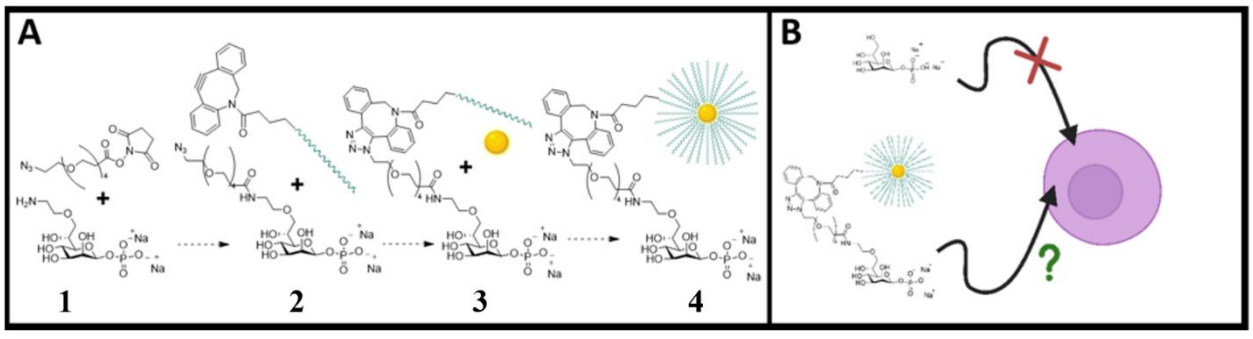

Figure 1. Panel A: Organic synthesis of HMP-DNA-thiol conjugates. These were then functionalized onto gold nanoparticles to form SNAs. Panel B: Uptake and activity studies of β-HMP-SNAs in comparison to β-HMP using flow cytometry and IL-8 response measurement via ELISA

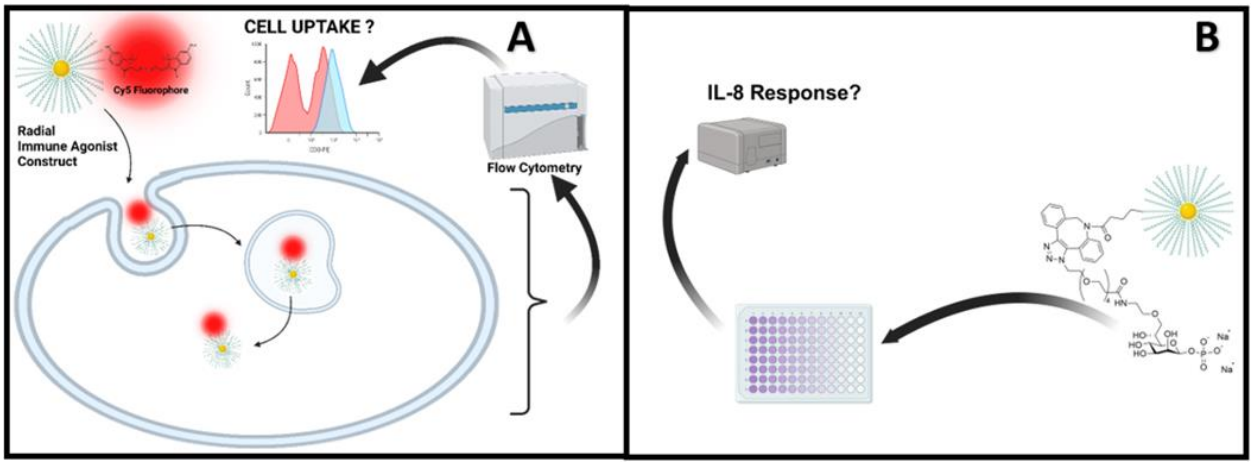

Figure 2. Cell uptake studies done using fluorescently labeled β-HMP-SNAs. Uptake will be analyzed using flow cytometry and confocal microscopy. Panel B: IL-8 response studies in which HMP construct is administered to HCT 116 cells. IL-8 response is measured using ELISA assay

Chapter 1: Introduction to Heptose Phosphates

1.1 Biological relevance of heptose phosphates

HMP, HBP, and ADP-Heptose are intermediates from the bacterial ADP-Heptose biosynthetic pathway.[1] Unique bacterial carbohydrates of this type are of particular interest, especially for adjuvant development due to their ability to function as PAMPs. PAMPs are molecular motifs produced by microbes that are recognized by pattern recognition receptors. Subsequently, this leads to host immune activation. Adjuvants are molecules that modulate the human immune response, which is desirable when trying to increase immunity to a disease. Adjuvants can be applied in the attempt to treat disease as seen in the HIV Kick and Kill approach. In pathogenic bacteria the ADP-Heptose biosynthetic pathway contributes to the generation of lipopolysaccharides, many of which are highly immunogenic. HMP, HBP, and ADP-Heptose from this pathway induce immune activation, while intermediates S7P and HMP-7 do not. The difference in activity between these two groups are due in part to the anomeric β-phosphate group as shown in Figure 3.[1]

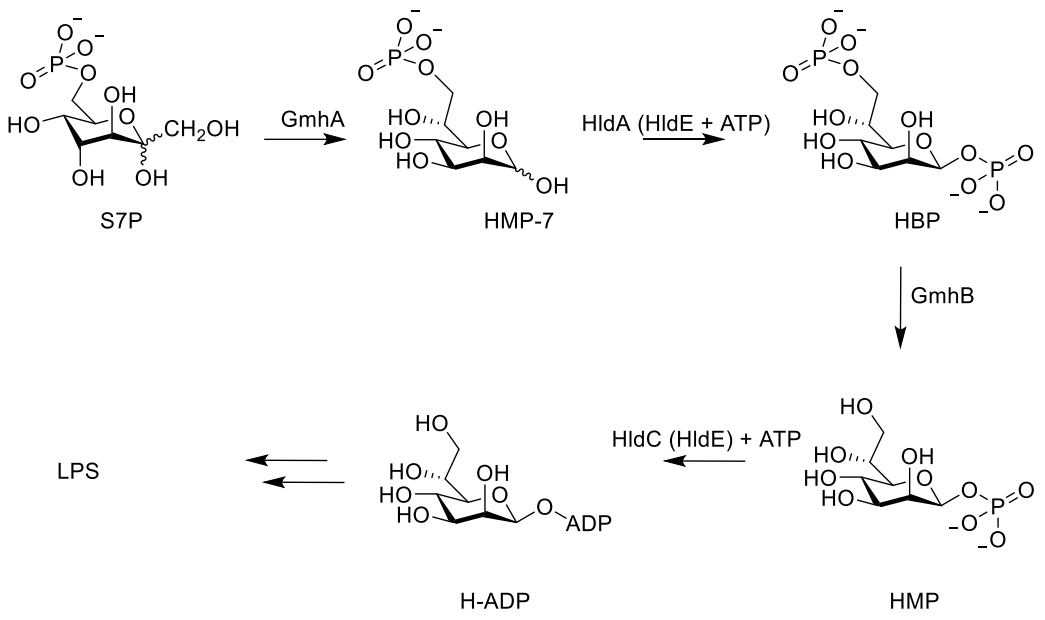

Figure 3. ADP-Heptose biosynthetic pathway involved in LPS generation in neisserial species

PAMPs have a long history of being effective adjuvants.[2] For example, CpG oligonucleotides are PAMPs that are agonists of TLR9 and have been used as adjuvants in the *Leishmania* vaccine candidate.[3–6] PAMPs have the ability to improve the effectiveness of an immune response.[7] An antigen-specific immune response could be modulated and optimized by using a PAMP, which would provide a pathway to more effective treatments.[7] If these heptose phosphates can generate a biologically relevant immune response, they may be considered for use in multiple therapeutic applications including addressing latency HIV-infected cells, as a vaccine adjuvant, or in cancer immunotherapy.[1,8–10]

1.2 Clinical relevance of HMP

As of 2022, 39 million people worldwide are living with HIV.[11] In contrast from the early 1980s, there now exists multiple treatments that enable people living with HIV to live long and healthy lives. These treatments are called antiretrovirals (ART)[11]. ART treatments can be

composed of integrase, nucleoside reverse transcriptase, non-nucleoside reverse transcriptase, and protease inhibitors[12]. Without reliable access and treatment, HIV infection will progress and lead to AIDS. Although, available and highly effective treatment are available there remains possible health concerns due chronic drug exposure, challenge of obtaining medication when a refill is needed, and the high cost of these life-saving drugs.[13]

At the time of the writing of this thesis, there is not a cure for HIV. Through adherence to treatment plans, individuals can suppress the viral load in their body. With an adequate level of suppression that is observed it becomes impossible to transmit HIV through sex[14]. It is key to note that stopping the treatments would cause viral rebound and disease progression would begin once again.[15] For this reason, among others it is in the best interest of the public to develop a cure for HIV.

The Kick & Kill strategy is an approach to eliminate HIV that is currently being developed.[16] This approach uses LRAs to increase HIV transcription and viral protein expression. The theory is that when virions are expressed in latently infected cells after activation with a LRA(Kick step), infected cells can be eliminated via immune-mediated clearance (Kill step).[16]

We know that HMP activates NF-kB and that NF-kB is hijacked by HIV so it transcribes viral proteins.[1,17] Thus HMP could potentially be a LRA.[18,19]

1.3 Nomenclature and classification of heptose phosphates

Heptose phosphates are exogenous to mammals and are produced in most Gram-negative bacteria such as *Neisseria gonorrhoeae.*[20] These molecules are intermediates from the biosynthesis of lipopolysaccharides.[20] D-glycero-β-D-manno-heptopyranose phosphates (Figure 4) are seven

carbon atom carbohydrates that are interesting because of the possibility that they can be used as immune agonists or adjuvants. Carbohydrates are defined as polyhydroxy aldehydes (H-[CHOH]$_n$-CHO) or polyhydroxy ketones (H-[CHOH]$_n$-[CHOH]$_m$-H) with at least three carbon atoms.[21] The relative configuration of stereogenic centers in aldose sugars are described in groups of up to four stereogenic centers, starting with the group that is adjacent to carbon one (Figure 5).[21] The heptoses in Figure 4 demonstrate the relative stereochemistry of mannose exists at the reducing end while a single stereocenter (glycerol) exists at the non-reducing end.

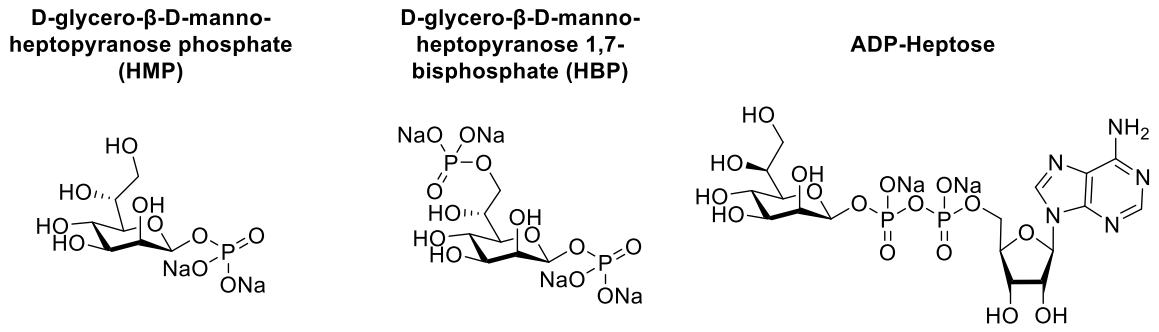

Figure 4. Heptose phosphates as PAMPs

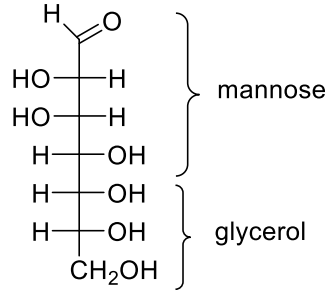

D-glycero-β-D-manno-heptopyranose

Figure 5. Fisher projection of D-glycero-β-D-manno-heptopyranose

The absolute configuration of carbohydrate stereocenters is then described using the D and L stereochemical descriptors. These descriptors are part of the Fischer-Rosanoff nomenclature

convention, where the molecule is drawn in a Fischer projection with the highest oxidation state at the top and the carbon chain in a vertical line down. The substituents are then added to the chain and if the higher priority substituent is on the right side, it is given the D descriptor and if the substituent is on the left side, it is given the L descriptor. To apply these descriptors in carbohydrate nomenclature, the last stereogenic center (highest numbered center) from group of stereocenters described by the relative stereochemistry descriptor (such as manno) is used to set the absolute configuration of all the centers in the descriptor.[21] A final key stereochemical element remains in carbohydrates and is found at the anomeric center. This center has unique reactivity and can be found in either stereochemical configuration or under some conditions can interconvert (mutarotation). The α and β stereochemical descriptors are used to describe the two configurations of the anomeric center (C-1 in all aldoses) and isomers at this site are called anomers.[21] Thus the D-glycero-β-D-manno prefixes describe unambiguously all the stereochemical elements in this molecule.

These carbohydrates are labelled as heptoses since they are monosaccharides that have seven carbon atoms. These molecules were recently discovered to activate an immune pathway.[1,20] The activation is in part due to the anomeric phosphate being in the β-position. This discovery led to these heptose phosphates being classified as PAMPs.[22]

1.4 Synthetic approaches to heptose phosphates and derivatives

There has been a considerable amount of work completed regarding heptose phosphates, including ADP-Heptose, the subject was reviewed extensively.[23,24] Synthesis of heptose phosphates generally involve protection, elongation, phosphorylation, then are concluded with

total deprotection when using D-mannose as a starting material. In the syntheses published, there are variations such as how phosphorylations, elongations, and deprotections are performed.

Modified heptose phosphates can also be synthesized to improve cell uptake and facilitate conjugation with molecular probes.[23] For example, at the 7-*O*-position of D-glycero-β-D-manno-heptopyranose phosphate 6-membered to 12-membered alkyl chains were added to increase lipophilicity. The 7-*O* was modified to an azide.[23] Lastly, an aminoethyl group has been added to the 7-*O* position (Scheme 1).[23] The purpose of the handle was to serve as a location to add a molecular probe for further biological studies.[23]

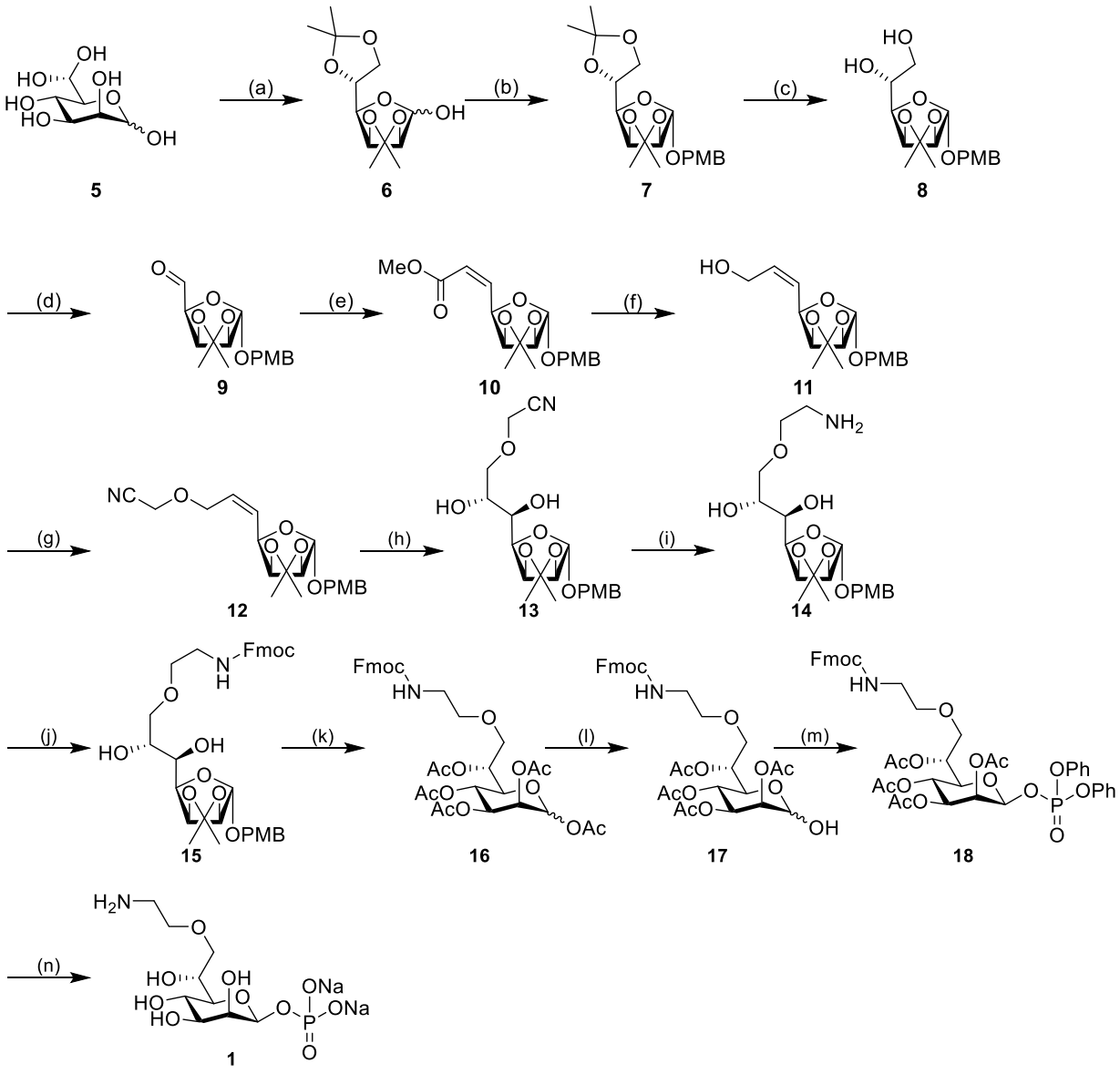

Scheme 1. Synthesis of aminoethyl-D-glycero-β-D-manno-heptopyranose phosphate.

(a)Acetone/$FeCl_3$, 16 h, 57%; (b) NaH, 4-Methoxybenzyl chloride (PMBCl), dimethylformamide (DMF), 1 h, 78%; (c) Acetic acid (AcOH), Water(4:1), 16 h, 99%; (d) Sodium periodate ($NaIO_4$), acetone/water (6:1), 0°C, 16 h, ; (e) $Ph_3PCHCOOMe$, toluene, 0°C, 2 h, 36% (over two steps); (f) Diisobutylaluminium hydride (DIBAL), dichloromethane (DCM), 0°C, 2 h, 40%; (g) Sodium hydride (NaH), bromoacetonitrile ($BrCH_2CN$), acetonitrile (ACN), 0°C, 5 h, 57%; (h)OsO_4, N-methylmorpholine N-oxide (NMMO), dioxane:acetone:water (1:2:1 v/v/v), 5 h, 51%; (i) BH_3-Me_2S (BMS), Tetrahydrofuran (THF), 80°C, 3 h; (j) Fmoc chloride (FmocCl), 16 h 46% (over two steps); (k) DCM:Trifluoroacetic acid (TFA):water, 0°C, 3 h, then Ac_2O:pyridine (1:1 v/v) 88%; (l) Hydrogen bromide (HBr)-AcOH, AcOH, DCM, 16 h, then CF_3SO_3Ag, Ag_2CO_3, 16 h, 58%; (m) $(PhO)_2P(O)Cl$, DCM, 4-Dimethylaminopyridine (DMAP), 2 h, 46%; (n) Platinum oxide (PtO_2), H_2, methanol (MeOH), 24 h, then Triethylammonium (TEA) Buffer, MeOH:water, 16 h 80%

The synthesis of the key 7-*O*-aminoethyl D-glycero-β-D-manno-heptopyranose phosphate is described (**4**, Scheme 1). It started with acetonide protection of the inexpensive D-mannose at positions C2, C3, C5, and C6 providing the expected product in 94% yield.[25] Following this, an anomeric protection was performed with PMBCl resulting in a globally protected carbohydrate in 78% yield.[26] C5 and C6 were deprotected using acetic acid and water. This deprotection afforded the desired product in 96% yield. Once deprotected, oxidative cleavage provided aldehyde **9**, which was used as is.[25] Treatment with methoxycarbonylmethylenetriphenylphosphorane ylide under typical Wittig reaction conditions elongated the aldehyde to produce methoxybenzyl (*Z*)-5,6-dideoxy-2,3-O-isopropylidene-α-D-lyxo-hept-5-enofuranoside and, methoxybenzyl (*E*)-5,6-dideoxy-2,3-O-isopropylidene-α-D-lyxo-hept-5-enofuranoside, as well as the by-product triphenylphosphine oxide. Unexpectedly, the formation of the *Z* configuration is favoured over the *E* configuration for these stabilized ylides due to the solvation phenomena participation from the C4 alkoxy group.[27] This phenomenon allows the preferential formation of the *Z*-product when using a stabilized ylide with carbohydrates when normally the *E* configuration would be expected.[27]

Ester **10** was then purified using flash chromatography resulting in a 60% yield over these two steps. After reduction with DIBAL, alcohol **11** was produced in 81% yield. Subsequently, the alcohol was alkylated using bromoacetonitrile in 88% yield. Dihydroxylation of alkene **12** produced methoxybenzyl-7-*O*-(cyanoethyl)-2,3-*O*-isopropylidene-D-glycero-α-D-manno heptofuranoside and methoxybenzyl-7-*O*-(cyanoethyl)-2,3-*O*-isopropylidene-L-glycero-β-L-gulo heptofuranoside. These diastereomers are formed because, during the dihydroxylation reaction, osmium tetroxide can approach from the top or bottom face of the alkene.[28] Depending on which

face is attacked, it will result in either the mannose or gulose derivative. The mannose derivative was separated from the gulose derivative by use of flash chromatography and recrystallization. This dihydroxylation afforded a yield of 65% of the desired mannose derivative.

Amine **14** was produced by using borane dimethyl sulfide to reduce the nitrile group. FmocCl was employed to protect the newly made amino group with a 60% yield over the reduction and protection.[29] Subsequently, the PMB and isopropylidene groups were removed and replaced with acetyl groups in 97% yield.[29] Interestingly, removal of the PMB group resulted in the formation of the pyranose sugar. Unlike the protected anomeric PMB glycoside, the C-1 hydroxyl group can undergo equilibration with the ring open sugar, which enables cyclization with the C-5 hydroxyl group from the dihydroxylation This converts the furanose ring into the pyranose. A deprotection followed by a phosphorylation was performed to provide the β-anomer preferentially with a 58% yield.[29]

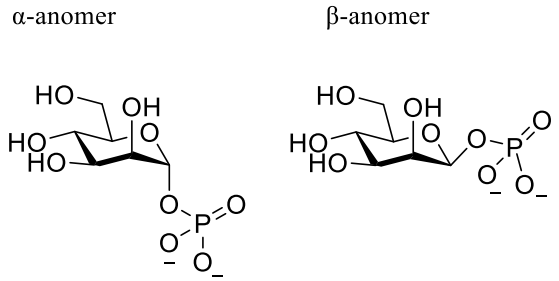

Figure 6. Anomers of mannose phosphate

Synthesizing the phosphorylated β-anomer is challenging due to the anomeric effect and steric hindrance of the axial C-2 hydroxyl, both of which favour the formation of the α-anomer (Figure 6). For α-D-mannose, there is back donation of the lone pair from the ring oxygen into the C-1 C-O σ* orbital that can only occur in the alpha configuration. This makes the α-glycoside more stable and thermodynamically preferred.[30,31] β-mannosides are quite difficult to generate

since the endo-anomeric effect favours the α-anomer and achimeric assistance from a participating C-2 protecting group also favours the α-anomer.[32] Thus obtaining phosphorylated β-anomers is challenging, particularly in light of the lability of the anomeric phosphate.[33] The β-anomer is required as it exhibits the desired biological activity, while D-glycero-α-D-mannoheptose-7-phosphate is not.[1] Starting from a lactol mixture of anomers that favours the α-anomer, Borio et al. report selective synthesis of the β-phosphate.[33] The minor β-lactol is more nucleophilic and thus reacts quickly. While the lactols are sensitive to DMAP mediated mutarotation, the phosphate is not. Thus DMAP in the reaction mixture equilibrates the α-anomer into a mixture of α- and β-anomers, where the more nucleophilic β-anomer can then be preferentially phosphorylated by the slow addition of diluted phosphorylating agent, DPPC.[33] The resultant major product, the β-anomer, was purified from the minor biologically inactive α-anomer. Total deprotection was then achieved with a yield of 62%. This resulted in the amine becoming available for conjugation and a biologically active heptose phosphate.[18]

1.5 Improving the cell uptake of heptose phosphates

HMP is not a suitable drug candidate because it is too hydrophilic and thus cannot effectively cross the cell membrane. To address this issue, the carbohydrates have been conjugated with aliphatic groups and/or linkers for transit via alternative pathways. Target molecules that transit through the plasma membrane need to possess appropriate characteristics based on their mechanism of action. HMP engages an intracellular target, ALPK1, and thus requires sufficient hydrophobic character to traverse the cell membrane and localize in the cytoplasm.[34,35] The drug candidate must therefore be sufficiently hydrophobic and maintain appropriate hydrophilic character to remain soluble in aqueous solution.[36] This is often difficult to achieve with

carbohydrates due to their polar hydroxyl groups. A common strategy to address this consists of making a prodrug in which the polar groups are protected with non-polar groups until they reach the desired location in the cell.[37] Formulations can also be developed such as liposomes that will aid in the delivery of compounds into the cell over various periods of time.[38]

Efforts have been made to improve cell uptake of heptose phosphates. Phosphates have been equipped with isoprenoid groups and nucleotide sugars.[39] The incorporation of an isoprenoid group makes it easier in principle for it to transit through the cell membrane.[40] In the case of a nucleotide sugar, there lies an opportunity to undergo active transport or at minimum uptake or translocation as alluded to in Pfannkuch et al.[41] Vincent et al. reported the use of non-hydrolyzable phosphonate analogues, where some were fluorinated at the carbon of the phosphonate while maintaining biological activity.[42] To increase lipophilicity of the compound, alkylation of the 7-*O* position with alkyl chains ranging from C_4 to C_{10}, and aminoethyl linker was performed.[23] The motivation of the alkylation is much like the addition of the isoprenoid group. The addition of the aminoethyl linker provides the opportunity to attach molecular probes. Azidation serves the same purpose as the aminoethyl group although by use of strain-promoted azide-alkyne cycloaddition (SPAAC) chemistry.[43] The results of these modifications to HMP were mitigated. Alkylation of HMP resulted in poor solubility in aqueous solution and difficulty in ion-exchanging triethylammonium for a sodium ion using Dowex-Na.[23] HMP with an aminoethyl linker required PtO_2 with platinum from specific sources to achieve deprotection of the anomeric phosphate.[23] Copper-catalyzed azide-alkyne cycloaddition facilitated conjugation of HMP to biotin. However, an oxidative side reaction would also produce biotin sulfoxide potentially leading to diminished function of biotin.[23,44]

1.6 Nanoscale formulations as a novel approach to deliver heptose phosphates

In contrast, nanoscale formulations, such as encapsulation within liposomes, present the advantage of facilitating delivery without the requirement for chemical modifications.[38] However, while liposomes are very effective for delivery to immune cells, they have a limited scope of tissues and cell types they can target. One nanoscale delivery approach that has shown consistent cellular uptake is the spherical nucleic acid (SNA) platform developed by Chad Mirkin in 1996. SNAs consist in a nanoparticle core that is functionalized with radially oriented oligonucleotides.[45] In this architecture, they have shown robust unaided cellular uptake in more than 50 cell types.[46] SNAs have also been formulated to facilitate the delivery of biomolecules previously (e.g., proteins, peptides, RNA), showcasing their relevance for the delivery of a glycan-based drug.[47–49] HMP which is a PAMP, faces challenges regarding cell uptake. By conjugating it to SNAs, we hypothesize that this will be an accessible strategy to increase its cell uptake.

More specifically, oligonucleotides are short strands of DNA or RNA that are generally less than 100 bases long. They are usually made using automated solid-phase synthesis using phosphoramidite chemistry.[50] Using this approach, oligonucleotides are synthesized one base at a time with precise control. Moreover, phosphoramidite building blocks can be incorporated that enable the addition of non-natural building blocks such as fluorophores (e.g., cyanine 3 and 5), click chemistry groups (e.g., DBCO, alkynes) and other groups relevant for bioconjugation (e.g., amines, thiols), making them versatile building blocks (Figure 7).

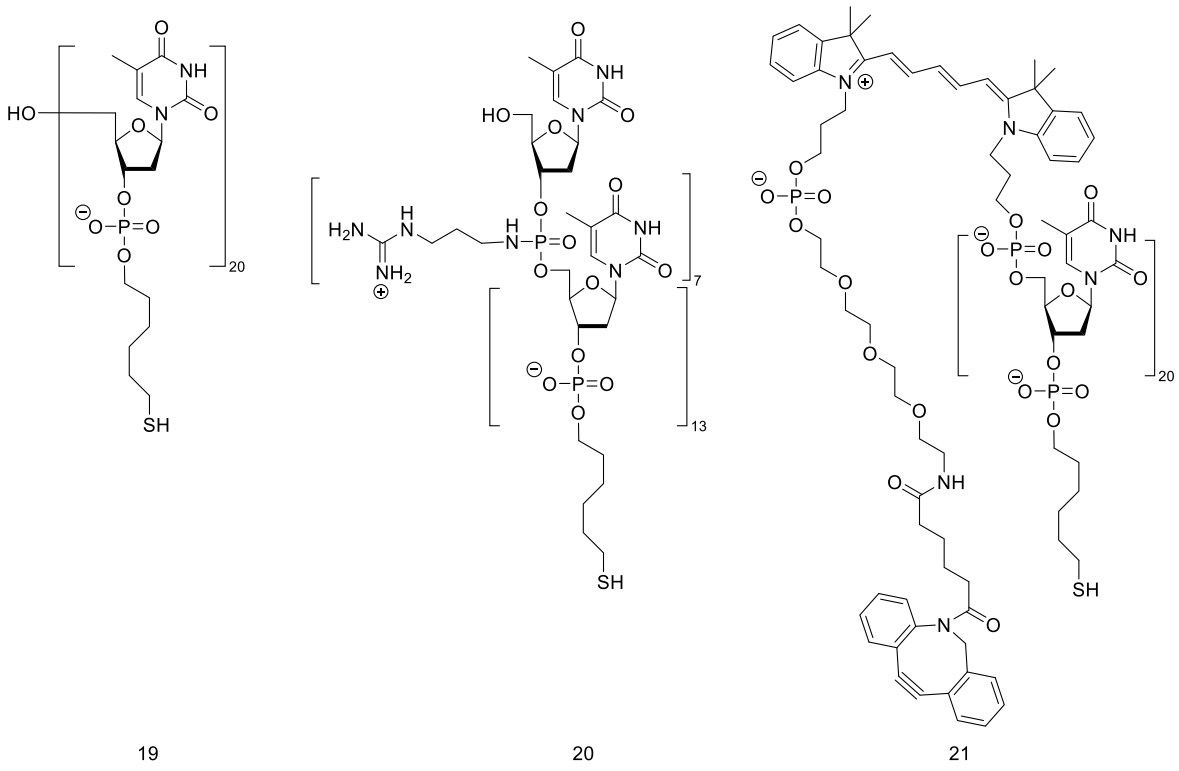

Figure 7. Oligonucleotides were used in this project.[Error! Reference source not found.] T20 (**19**), 5'-Guanidinium (GUA)7-T13-SH-3' (**20**), and 5'-DBCO-Cy5-T20-SH-3' (**21**)

Most oligonucleotides used in a therapeutic context aim to interact with their targets via Watson-Crick base-pairing to modulate gene expression.[51] However, oligonucleotides present unique potential as materials because they are programmable, biocompatible and water soluble.[52] For example, in the SNA architecture, they become a drug delivery vehicle, which utilizes oligonucleotides to aid in the delivery of therapeutics.[45] In this architecture, they present emerging properties that improve on linear oligonucleotides. For example, this dense functionalization sterically hinders nuclease degradation, thus providing an increased level of stability.[46,53]

The first synthesis of a SNA involved the dense functionalization of a gold nanoparticle core with oligonucleotides functionalized with a thiol group. (Figure 8. Panel A: Synthesis of dual-

layer SNA). A salt-aging process was used to maximize the DNA loading onto the nanoparticles, which aided in shielding the repulsive electrostatic interactions from the negative charges on the phosphate backbone. [7] Gold nanoparticle cores were used in this work because they are easy to synthesize and characterize via UV-visible spectroscopy from their plasmon resonance band at 520 nm. They are also stable at room temperature and can be readily functionalized with molecules presenting thiols under mild conditions.

Of particular relevance to this work is the finding that SNAs can achieve cellular uptake without the need for transfection agents.[46,54] More specifically, the mechanism for cellular uptake of SNAs has been elucidated and found to rely on recognition by scavenger receptors of type A followed by endocytosis (Figure 8. Panel A: Synthesis of dual-layer SNA. Panel B: Caveolin-mediated endocytosis of SNAs).[55] The pathway for endocytosis of an SNA does not require cationic transfection reagents that overcome coulombic repulsive forces as ssDNA does. Instead, it is the nanoscale architecture of the SNA that confers it the ability to undergo endocytosis.

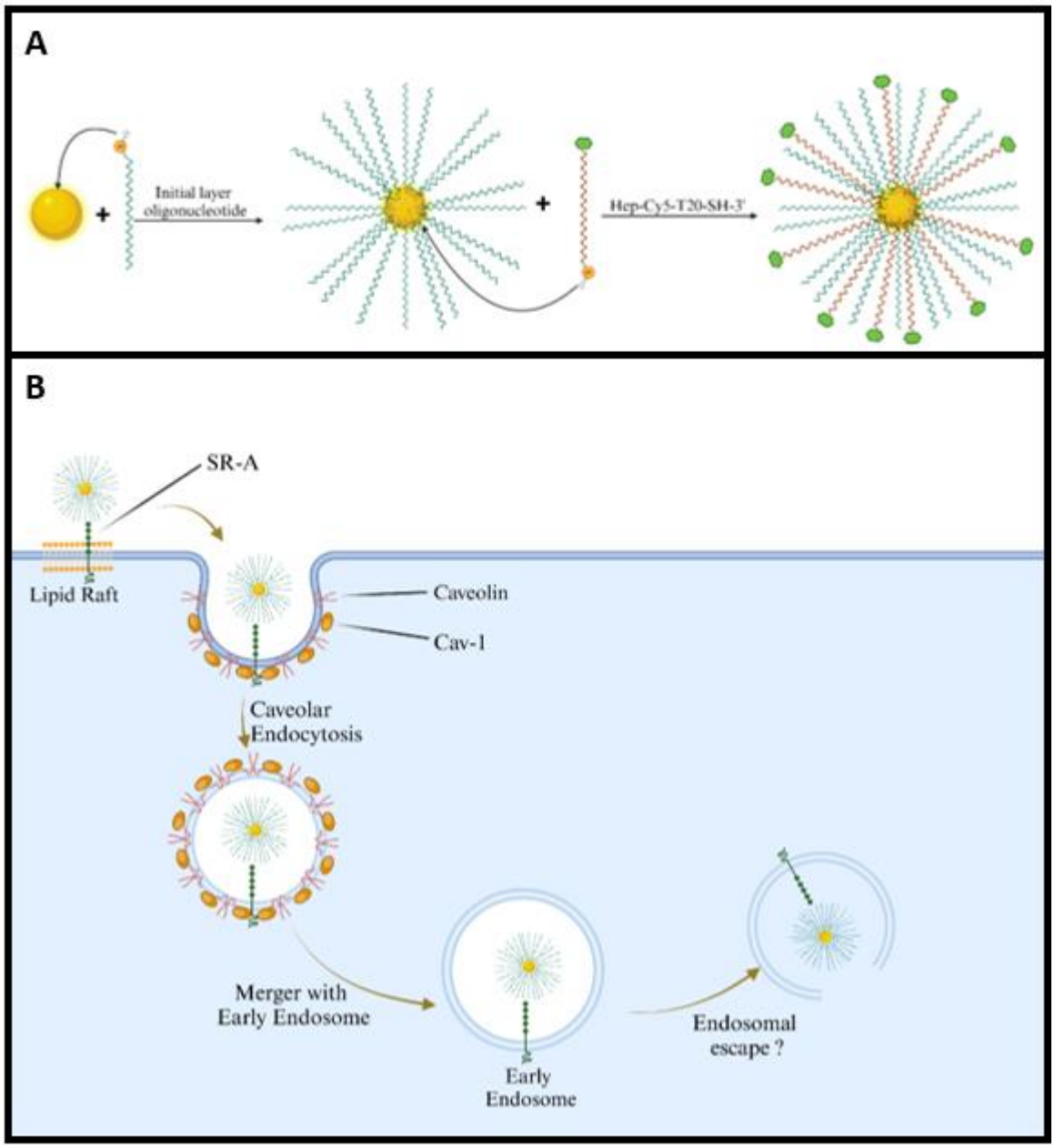

Figure 8. Panel A: Synthesis of dual-layer SNA. Panel B: Caveolin-mediated endocytosis of SNAs.

1.7 Adapting procedures from small molecule work to the nanoscale

In organic small molecule synthesis, molecules and the success of reactions are analyzed using nuclear magnetic resonance (NMR), and electrospray ionization-mass spectrometry (ESI-

MS).[56,57] These approaches allow close analysis of chemical bonds and their stereochemistry. However, it becomes more difficult to elucidate useful information from their spectra as molecules go beyond the 1000-1500 Da scale.

DNA is a larger molecule that cannot be easily analyzed by NMR, or ESI-MS. To analyze changes in the structure of oligonucleotides, polyacrylamide gel electrophoresis (PAGE) is used.[58] This form of analysis will visually display relatively large differences in mass (i.e. 300 Da), which correspond approximately to a single nucleotide addition and/or it can confirm if a conjugation has occurred. Matrix-Assisted Laser Desorption Ionization Mass Spectrometry (MALDI-MS) can determine the mass of oligonucleotides and help confirm their molecular structure (i.e. 1,000 Da to 300,000 Da) with better resolution than PAGE.[59–62] If high resolution is attained, carbon-13 resolution can be seen and help confirm the exact mass of the oligonucleotide, which may confirm small modifications (e.g., changes in functional groups, presence of protection groups, etc.).[63]

When determining concentrations with small molecules, it is usually sufficient to use a balance to weigh out material. When working oligonucleotides, the use of UV-visible spectrophotometers, such as the Nanodrop, is required to determine concentrations. Oligonucleotides are typically prepared in sub milligram amounts (μmol to nmol) that are best determined by spectrophotometers. They also present a characteristic absorbance at 260 nm, which enables their quantification using extinction coefficient derived experimentally and from mathematical models using Beer's law.

Chapter 2: Results and Discussion

2.1 Synthesis of aminoethyl-D-glycero-β-D-manno-heptopyranose phosphate

The synthesis of aminoethyl-D-glycero-β-D-manno-heptopyranose phosphate was performed as previously described.[29] D-mannose was first protected at positions C2, C3, C5, and C6 in 57% yield as in prior literature (Figure *9*).[29,64] The product was confirmed when the acetonide protons (~1.5 ppm) were identified via NMR. Protecting aforementioned positions was pursued to enable targeted deprotection of C5 and C6. The yields obtained were lower than what was reported in literature. Performing the reaction at a larger scale is the suspected reason for lower yields. It is documented that when scaling up reactions from small (milligram) to pilot scale (multiple grams+) yields can be lower and require additional methods to control temperature and mixing, two reaction features that do not scale linearly.[65,66]

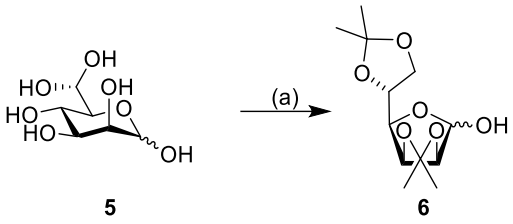

5 **6**

Figure 9. Acetonide protection. Condition (a): Acetone/$FeCl_3$, RT, 16 h, 57%

The anomeric carbon was protected using PMBCl, with a moderate yield of 61% while Sauvageau et al. obtained a 78% yield (Figure *10*).[29] The product was confirmed by the presence of aromatic protons close to 7 ppm. Anomeric protection was pursued to prevent alkylation in a later reaction. Going forward, improving the circulation of the water bath may help increase yield by ensuring a constant temperature.[66]

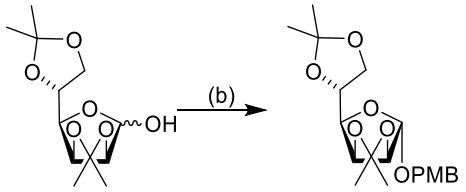

6 7

Figure 10. Anomeric protection. Condition (b): NaH, PMBCl, DMF, RT, 1 h, 61%.

C5 and C6 were deprotected with a solution of glacial acetic acid and water at RT. C5 and C6 then underwent oxidative cleavage using sodium periodate in acetone and water, which provided the desired aldehyde in 88% yield. While this remains efficient, it is not as high as the 96% yield previously reported (Figure *11*).[29] The product was identified by ^{1}H NMR analysis that displayed a reduction in the number of protons present in the acetonide region. Selective deprotection and oxidative cleavage was pursued to prepare for elongation of the carbohydrate. Future reactions would likely benefit from the use of slightly more acetic acid.

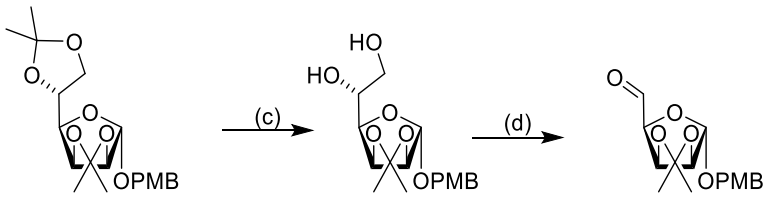

7 8 9

Figure 11. C5,C6 deprotection and oxidative cleavage. Condition (c): AcOH/water (4:1), RT, 16 h. (d) $NaIO_4$, acetone/water (6:1), 0°C, 16 h, 88%

The Wittig reaction was then performed, and the resulting products were purified using flash chromatography which provided the product in 36% yield (Figure *12*). The yield was low in comparison to the 90% yield reported by Brimacombe et al.[67] Formation of the product was confirmed via ^{1}H NMR. Protons in the alkene region were observed with a coupling constant of

11 Hz which is indicative of the desired *Z*-product. *Trans* alkenes have different dihedrals angle, which lead to coupling constants around 15 Hz in the context of this intermediate.[67] This step was done to add a carbon thus elongating the intermediate. Triphenylphosphine oxide, the by-product of the Wittig reaction, caused difficulties during purification. Without adequate warming while concentrated prior to flash chromatography, rapid crystallization occurs. This happened while loading into the silica gel cartridge and prevented further addition of the solution. The purification was achieved, although it required more cartridges than anticipated and lead to reduced yields. Going forward, better temperature management is needed, along with more dilute mixtures prior to performing flash chromatography.

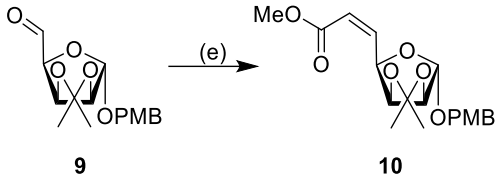

9 **10**

Figure 12. Wittig olefination. Condition (e): $Ph_3PCHCOOMe$, toluene, 0°C, 2 h, 36%

The carbohydrate ester **10** was then reduced, which yielded the expected alcohol in 40% yield (Figure *13*). The structure was confirmed by ^1H NMR that the product was synthesized due to the loss of a peak that corresponded to methyl ester protons, which occurred around 3.8 ppm in the starting material. In comparison, an 81% yield was reported in literature.[29] In this step the ester is reduced to provide an alcohol, which will serve as alkylation site for the aminoethyl handle. Substantial amounts of aluminum salts, which formed a gel may have prevented effective extraction of the product during work up resulting in lower yields. Going forward, the gel will be separated into portions to enable effective extractions with glass wool.

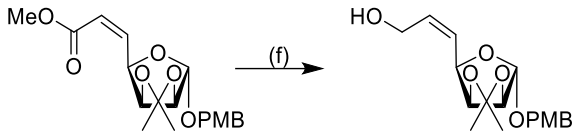

10 **11**

Figure 13. DIBAL reduction. Condition (f): DIBAL, DCM, 0°C, 2 h, 57%

The resulting free hydroxyl was then alkylated with bromoacetonitrile generating the expecting ether in 57% yield (Figure *14*). The product was confirmed through NMR. At around 4.2 ppm the integration increased from 1 to 3, which accounts for the protons next to the nitrile group and alkene. Alkylation of the free hydroxyl in literature attained an 88% yield.[23] Alkylation of this hydroxyl was the first step to permitting linkage between the carbohydrate and the intended oligonucleotide. A reason for the difference in yield could be due to the concentration of starting materials.[68] Regarding concentrations it was observed when operating on a concentration of 0.2 M of alcohol **11**, yields were substantially lower. When the reaction was done with a concentration of 0.23 M the highest yields in this work were obtained. Concentrations as high as 0.39 M provided suitable yields relative to the work done in this study. To improve yields from this reaction in subsequent works different concentrations could explored.

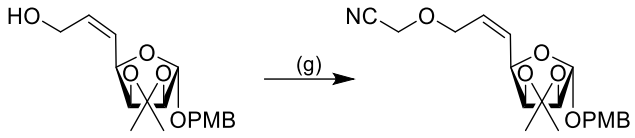

11 **12**

Figure 14. Bromoacetonitrile alkylation. Condition (g): NaH, bromoacetonitrile, ACN, 0°C, 5 h, 57%

Methoxybenzyl-7-*O*-(cyanoethyl)-2,3-*O*-isopropylidene-D-glycero-α-D-manno-heptofuranoside and methoxybenzyl-7-*O*-(cyanoethyl)-2,3-*O*-isopropylidene-L-glycero-β-L-gulo were obtained after dihydroxylation (Figure *15*). Both carbohydrates were separated using flash

chromatography, affording a yield of 51% of the D-glycero-α-D-manno derivative. In literature yields of 65% yield for the same dihydroxylation have been attained.[23] A coupling constant of 6.4 Hz for H5 was observed in the ^{1}H NMR that is consistent with literature data.[23] Dihydroxylation provides the provides the D-glycero-α-D-manno heptose moiety necessary for desired biological activity.

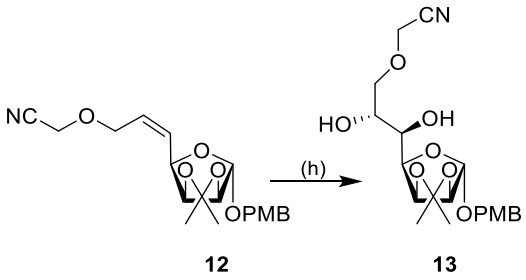

Figure 15. Dihydroxylation. Conditions (h): OsO_4, NMMO, dioxane:acetone:water (1:2:1 v/v/v), RT, 5 h, 51%

Reducing the nitrile with borane dimethyl sulfide complex led to an amine capable of conjugation. The amine was then temporarily protected using fluorenylmethoxycarbonyl in a moderate yield of 47% over two steps when compared to the 60% yield previously reported (Figure *16*).[23] Drying the carbohydrate derivative overnight and adding 5 equivalents of borane dimethyl sulfide complex may improve yields going forward. Using NMR, it was determined that the product had been isolated, as seen by an increase in protons in the aromatic region (7–8 ppm) indicating the fluorenylmethoxycarbonyl group is present.

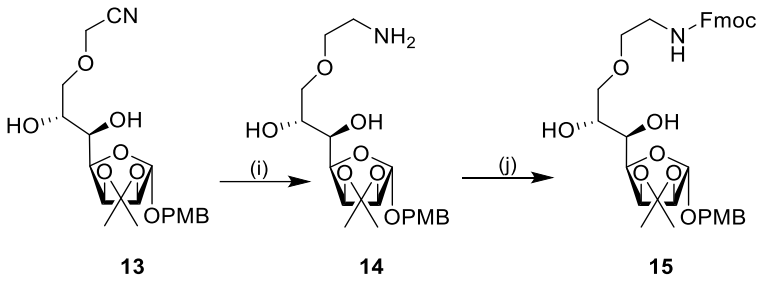

Figure 16. Nitrile reduction and Amine protection Conditions: (i) BMS, THF, 80°C, 3 h; (j) FmocCl, RT, 16 h, 47% (over two steps)

Using TFA, the acetonide and PMB protecting groups were removed. Acetic anhydride was then employed to acetylate the intermediate providing a slightly lower yield of 88% in comparison to the 97% from literature (Figure *17*).[23] In this step, deprotection of C1 enabled the iosmerization of the furanose to the pyranose intermediate via the open chain aldehyde. The reason for the decreased yield could be due to incomplete removal of water. Residual water would hydrolyze acetic anhydride. Acetylation of the carbohydrate would be insufficient and result in a lower yield. To improve yields going forward, prior to global protection, the carbohydrate will be placed under high vacuum for 1h. Using NMR, the loss of signal for the methylene protons in the PMB group (3.8 ppm) and the increase of methyl protons from the acetate groups (2.2-1.8 ppm) indicated a successful reaction.

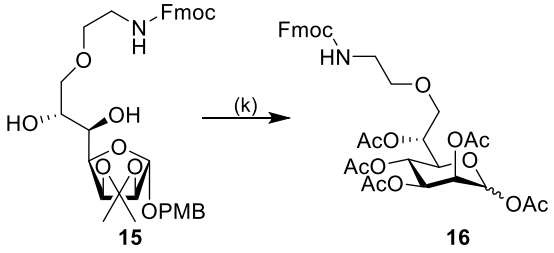

Figure 17. Partial deprotection and protection. Condition (k): DCM:TFA:water, 0°C, 3 h, then Ac_2O:pyridine (1:1 v/v), RT, 16 h, 88%

Subsequently, anomeric deprotection was performed, providing a moderate yield of 50% while yields of 84% were reported (Figure *18*).[23]This targeted deprotection prepared the intermediate for phosphorylation. Going forward using more equivalents of acetic acid and placing the carbohydrate under high vacuum overnight may help to increase yields.

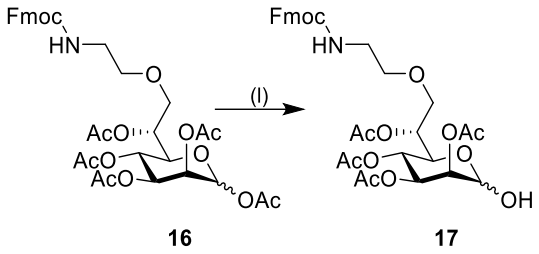

Figure 18. Anomeric deprotection. Condition (l): HBr-AcOH, AcOH, DCM, 16 h, then CF_3SO_3Ag, Ag_2CO_3, RT, 16 h, 50%

Next, the phosphorylation using DPPC and DMAP attained a lower yield of 45% in comparison to the 58% yield recorded in literature (Figure *19*).[23] This afforded the β-anomer after separation via flash chromatography from the α-anomer. The β-anomer was confirmed by the H1 doublet at 5.65 ppm as previously reported.[23] During the phosphorylation, the yield was influenced by the rate of addition of DPPC. Slow addition was crucial to preferential production of the β-anomer. Phosphorylation in this step was done to enable biological activity in the final product. Slow addition of the phosphorylating agent under conditions favoured the β-phosphorylated product as discussed in literature.[23,33] Going forward making more dilute mixtures of DPPC should increase the yield.

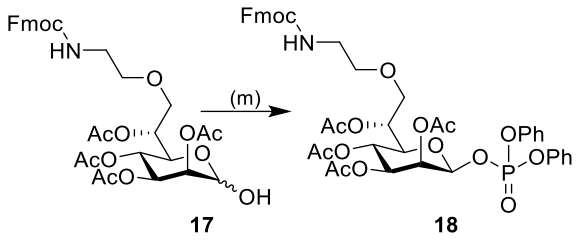

Figure 19. β-anomeric phosphorylation. Condition (m): $(PhO)_2P(O)Cl$, DCM, DMAP, RT, 2 h, 45%

Global deprotection was performed with PtO_2 (Millipore product #459925), triethylamine, methanol, and hydrogen gas bubbling through the mixture as described in literature to provide **1** with a significant yield of 80% in comparison to the 62% yield obtained in Sauvageau et al.[23] This final step, often required three or more iterations of deprotection to go to completion. However, excessive iterations with PtO_2 caused degradation. Thus, a balance between efficient deprotection and risk of degradation was needed to produce **1**. The molecule was produced due to the use of the particular PtO_2 (Millipore product #459925) which has a surface area of 75 m^2/g which is greater than at least one of the other batches that were tested in work by Sauvageau et al.[23] Having a larger surface area increases the number of accessible active sites present in regards to catalysts in general.[69] Using NMR, it was determined that all protecting groups were removed as indicated by lack of peaks in 7-8 ppm and 2.5-1.5 ppm region. As well, the coupling constant of H1 indicated that the correct anomer had been isolated. Removal of protecting groups and subsequent salt exchange provided the precursor molecule that is both active and ready for conjugation (Figure 20).

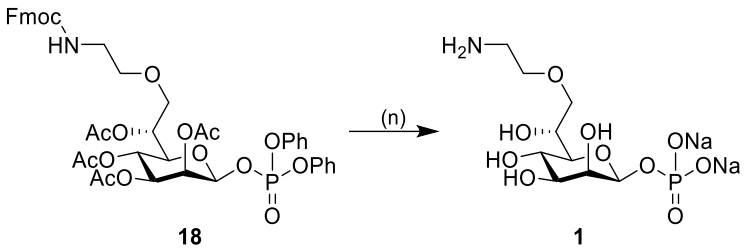

Figure 20. Total deprotection. Condition (n): PtO_2, H_2, MeOH, 24 h, then Triethylammonium (TEA) Buffer, MeOH:water, 16 h, 80% (over two steps)

2.2 Azido PEG4 NHS Ester Conjugation

To prepare for the conjugation with DBCO-functionalized oligonucleotide, the carbohydrate was reacted with azido-PEG4-NHS, ester which produced compound **2** in a 49% yield. **2** was achieved as a title compound and was purified using HPLC as shown in Figure 21.

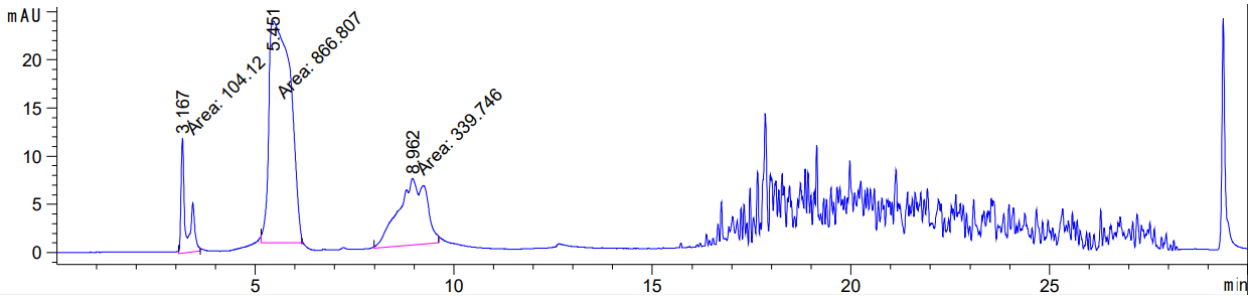

Figure 21. HPLC Trace of PEG4 Azide-7-*O*-(amidoethyl)-D-glycero-β-D-manno-heptopyranose phosphate. Product (**2**) isolated from peak three at 8.9 min

PEG4 Azide-7-*O*-(amidoethyl)-D-glycero-β-D-manno-heptopyranose phosphate (HMP-LINK, **2**) was purified by reverse phase HPLC. A gradient of 0% to 100% acetonitrile over 20 minutes was performed using a semi-prep Agilent Infinity 1260 HPLC. HMP-LINK, **2**, eluted at

8.9 min and this peak was collected. The noise that is seen towards the end of the chromatogram is related to running 100% acetonitrile for 10 minutes to wash out the remaining impurities from the column. The low concentration of HMP-LINK (**2**) used enabled the noise signal to be noticeable. The noise was due to organic contaminants eluting at 70%+ acetonitrile.

Because HMP-LINK, **2**, is the key reagent for further biological studies and a new compound in the literature, it was fully characterized. Mass spectrometry was performed to confirm the chemical formula of **2**. This molecule had an expected $[M+Na]^+$ *m/z* of 629.2042 Da. High-resolution Q Exactive Hybrid quadrupole Orbitrap mass spectrometer was used and found 629.2084 $[M+Na]^+$, confirming the chemical formula. The ^1H NMR was also consistent with this structure, showing pronounced peaks between 3.5 and 4 ppm that correspond to the protons from the ether regions of PEG4. Using COSY, HSQC, and HMBC, the ^1H and ^{13}C spectra could be fully assigned and were consistent with the structure of **2**.

2.3 Method Development for Oligonucleotide and SNA Conjugations

2.3.1 Conjugation of HMP-LINK with 5'-DBCO-Cy5-T20-SH-3'

Initial conjugation of HMP-LINK of oligonucleotides was performed with oligos received from McMaster University. 5'-DCBO-Cy5-T20-SH-3' (Scheme *2*) was treated with 100 equivalents of HMP-LINK in deionized water, at room temperature for 24 hours in the dark. This resulted in an unsuccessful conjugation (Figure 24). PAGE (Figure 22) and MALDI-MS (Figure 23) analyses were consistent with unreacted and partially degraded oligonucleotide starting materials. This data suggests that the DBCO group on the DNA had degraded.[70] A second batch of 5'-DBCO-Cy5-T20-SH-3' was received. The oligonucleotide was first assessed for quality using

UV-Vis spectroscopy. The characteristic DBCO UV-Vis peak at 310 nm was not observed suggesting that, the DBCO had again degraded (Figure 25).[71,72] We hypothesize that exposure to heat during transport resulted in oxidation and the addition of water to the alkyne (Scheme 3).[71,72] During transit from Hamilton to Ottawa, 5'-DBCO-Cy5-T20-SH-3' may have been subjected to conditions that resulted in an inactive DBCO group. Due to this challenge, we proposed that the next conjugation experiment should be performed at McMaster University (Scheme *2*).

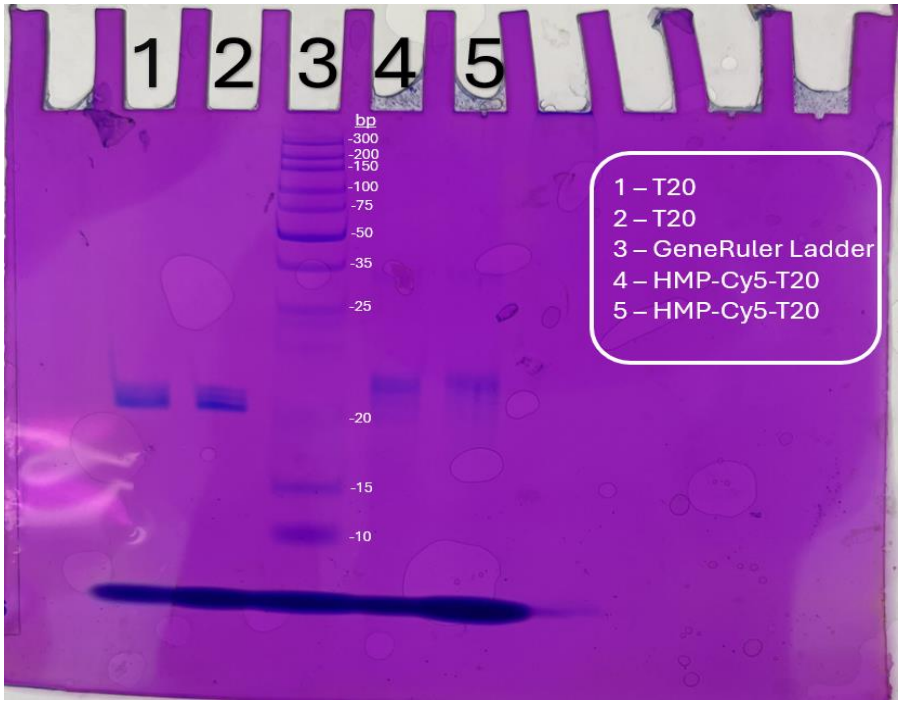

Figure 22. PAGE analysis using 19:1 Bis/acrylamide in 20% concentration to assess conjugation of β-HMP to oligonucleotides. Lanes 4 and 5 were failed reactions in which the conjugation did not occur

To validate that degraded DBCO was the cause of the unsuccessful conjugation, HMP-LINK was conjugated to an intact DBCO-containing molecule available in the lab (Figure *26*). From the reaction DBCO-PEG$_4$-triazole-PEG$_4$-acid was formed, and the results were assessed via LRMS (Figure 27). The reaction (Scheme *4*) was achieved using a 1:1 molar ratio of starting

materials in deionized water and DMSO (2:1, v/v) at RT for 1 h. LRMS detected a mass of approximately 1,159.8 Da confirming the reactivity of the azide (Scheme 4).

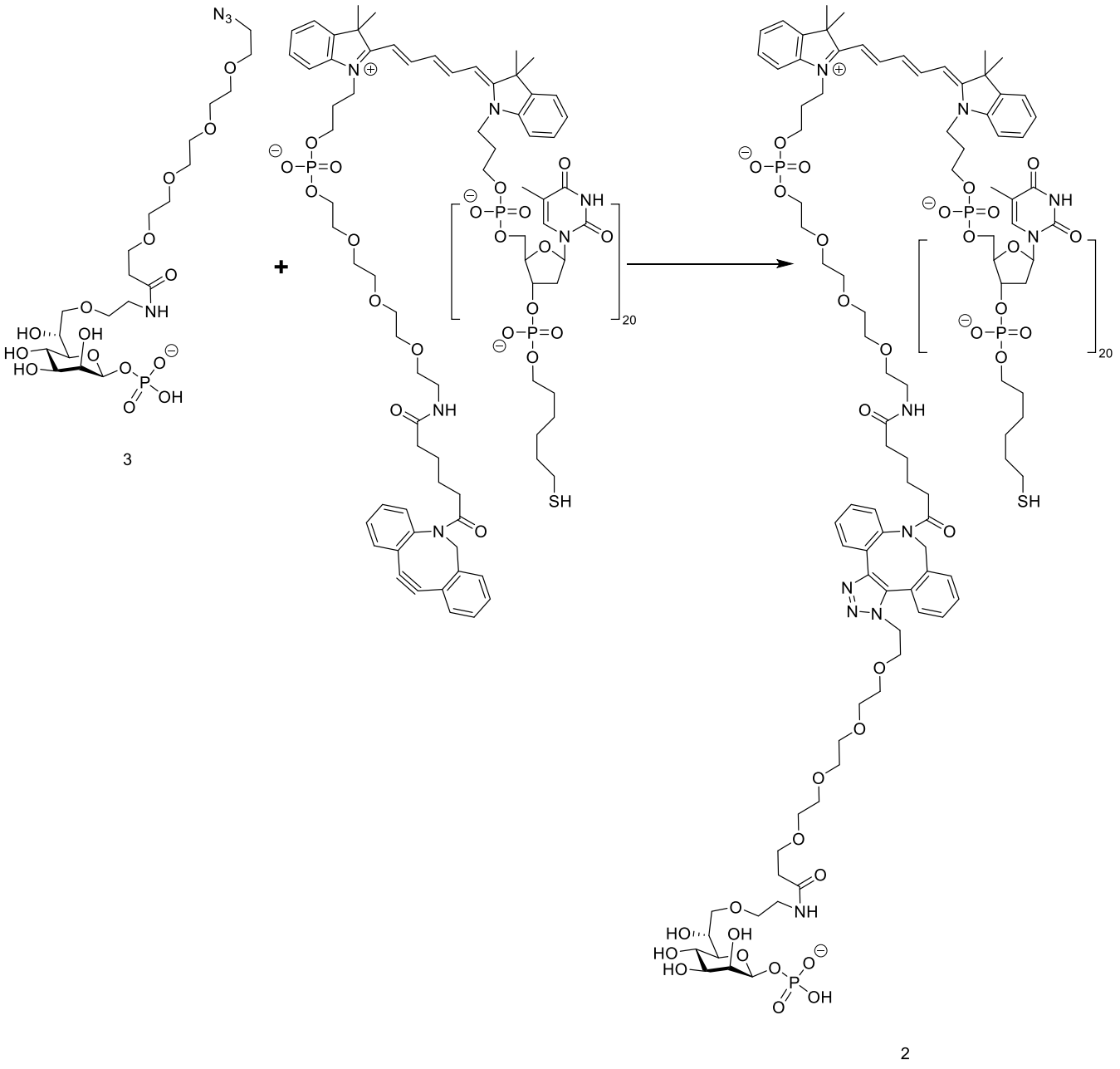

Scheme 2. HMP-LINK **2** to DBCO-Cy5-T20 conjugation

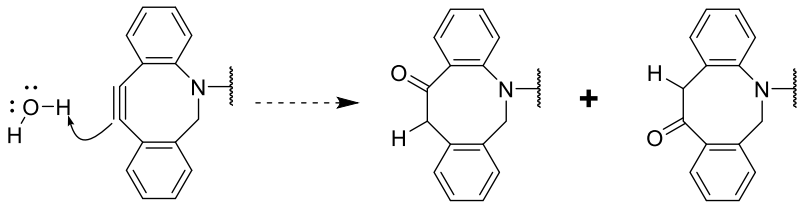

Scheme 3. Proposed products of DBCO-Cy5-T20 formed by oxidation and hydration of strained alkynes

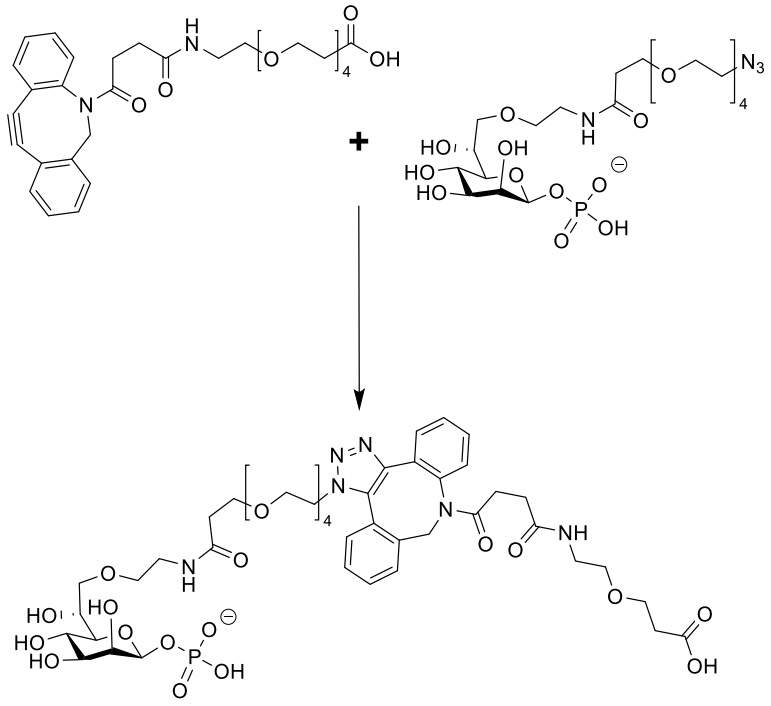

Scheme 4. The successful conjugation of HMP-LINK with DBCO-PEG$_4$-triazole-PEG$_4$-acid, as evaluated by MS, confirmed that the azide of HMP-LINK was reactive with DBCO .

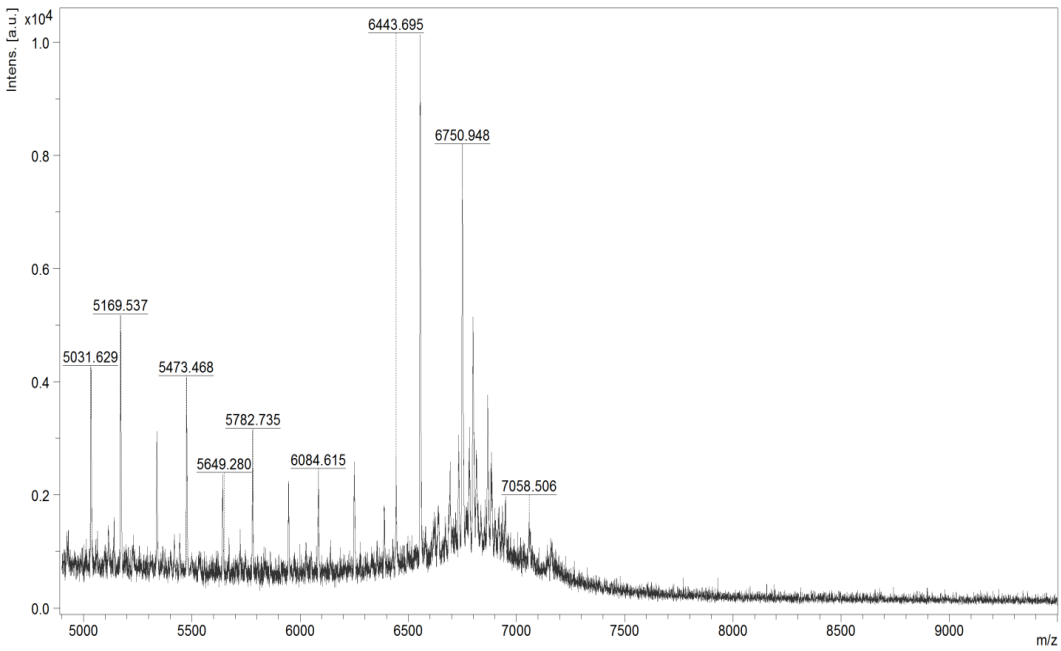

Figure 23. Degradation of unconjugated DNA found using DHAP as a matrix and MALDI analysis. Masses at: 6750.948 Da and 7058.506 Da correspond to 5'-Cy5-T20-SH-3' and 5'-DBCO-Cy5-T20-SH-3' respectively. Spectrum obtained using a Bruker ultrafleXtreme MALDI-TOF/TOF

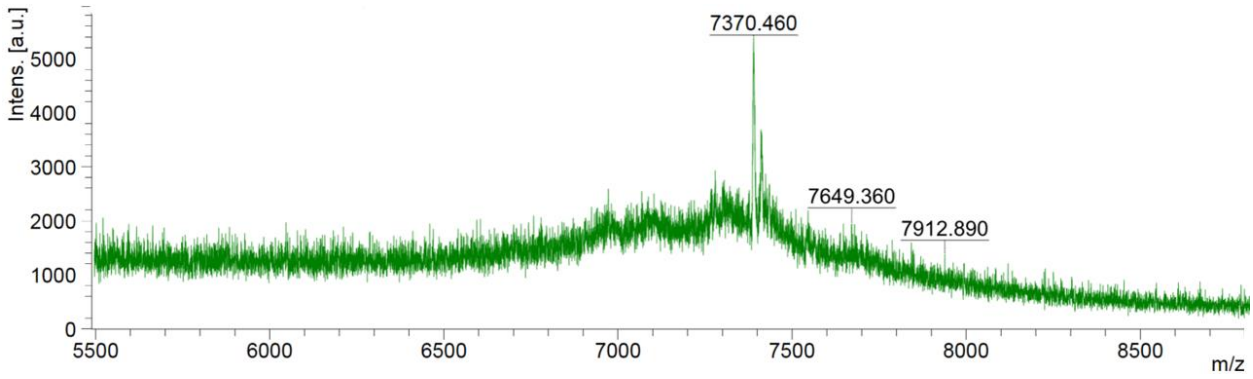

Figure 24. Assessment of attempted conjugation between DBCO-Cy5-T20 and HMP-LINK. Only DBCO-Cy5-T20 detected as shown by the key mass of 7370.460 Da. The expected product with a mass of 7 924.68 Da was not detected. Spectrum obtained using a Bruker ultrafleXtreme MALDI-TOF/TOF

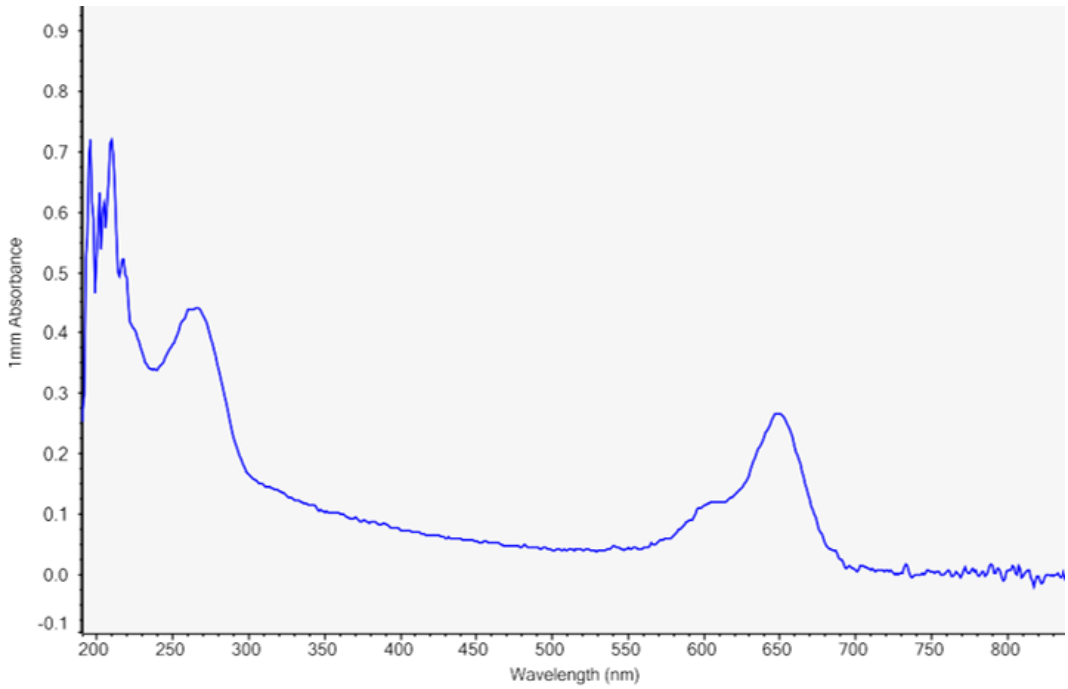

Figure 25. UV-Vis spectra of degraded 5'-DBCO-Cy5-T20-SH-3'. The expected absorption band for DBCO at 310nm is not present

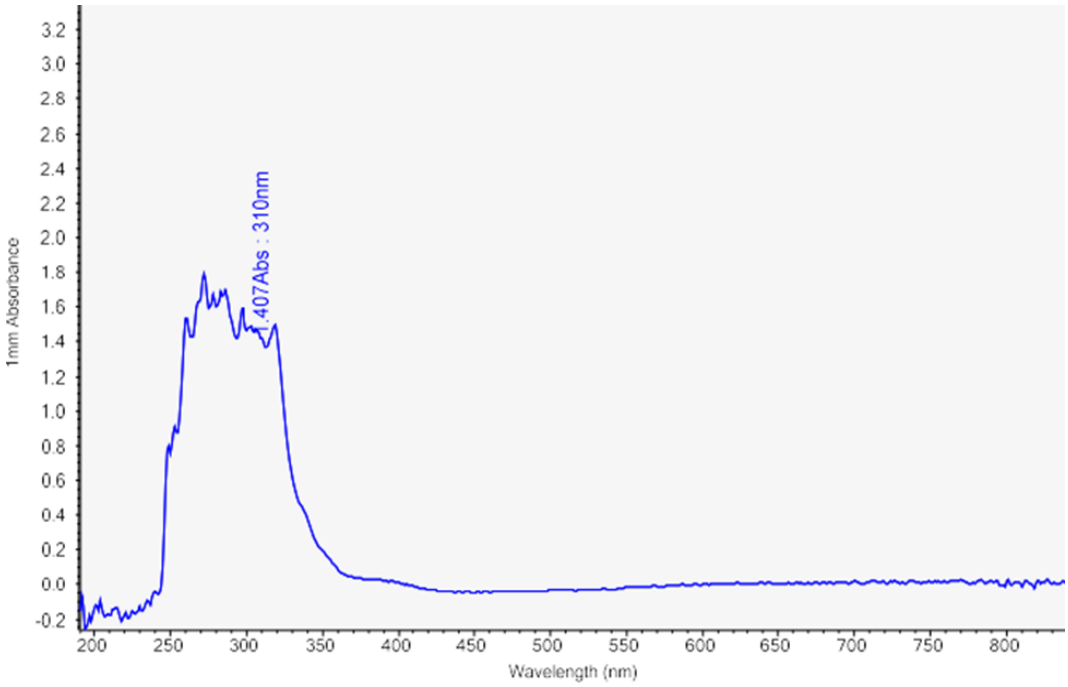

Figure 26. UV-Vis spectra of DBCO-PEG4-acid. The DBCO absorption peak can be seen at 310nm

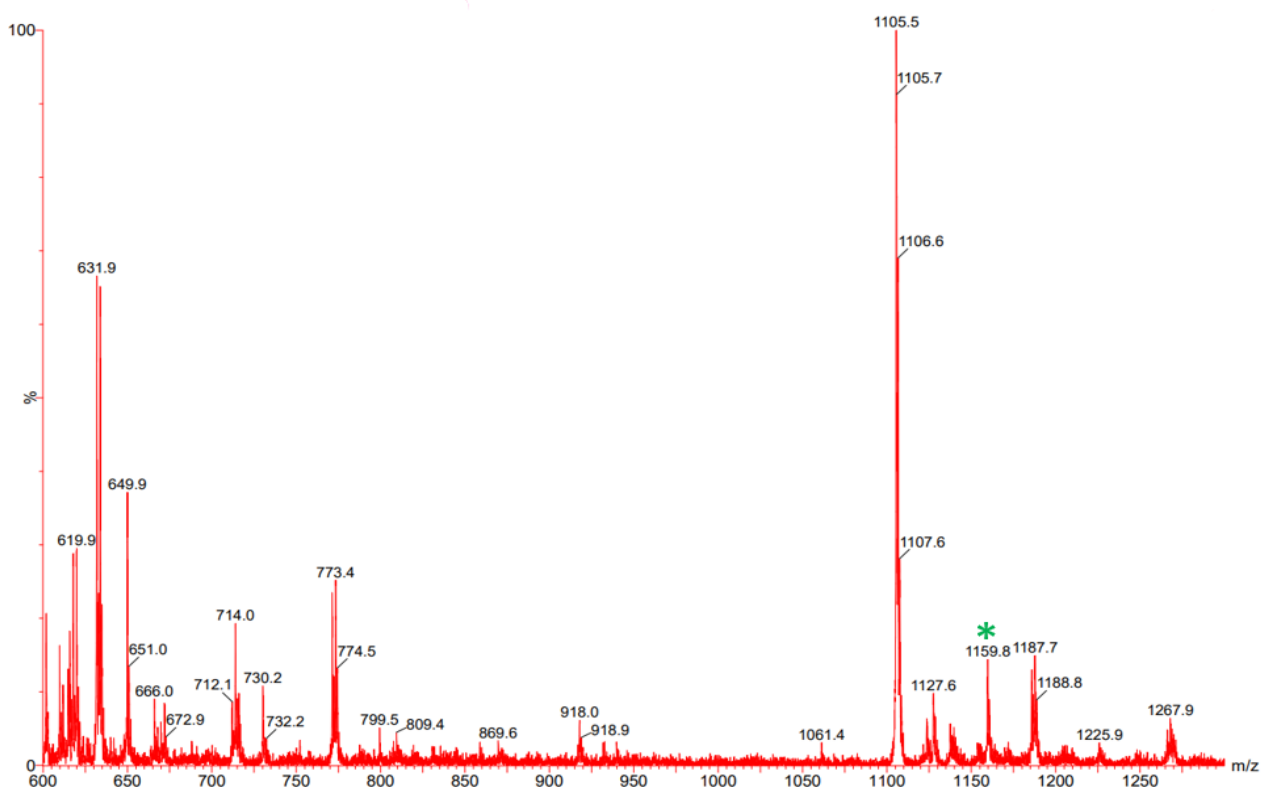

Figure 27. Mass Spectrum of test reaction product HMP-PEG8-acid. $C_{50}H_{76}N_6O_{23}P^+$; calc'd =1159.47 found $[M+H]^+$ = 1159.8

2.4 HMP-LINK conjugation to 5'-DBCO-Cy5-T20-SH-3' at McMaster University

To overcome the sensitivity of the DBCO functional group on the oligonucleotide, HMP-LINK was shipped to McMaster University and conjugated to 5'-DBCO-Cy5-T20-SH-3'. The reaction was found to be successful as seen in Figure 28 and Figure 29. PAGE analysis (Figure 28) demonstrates that 5'-HMP-Cy5-T20-SH-3' is formed because it did not migrate as far on the gel as the unreacted 5'-DBCO-Cy5-T20-SH-3' control, which indicates it has a larger mass. ESI-QTOF (Figure 29) aligns with PAGE analysis confirming that molecule **2** (Scheme 2, Figure 28) has been synthesized successfully.

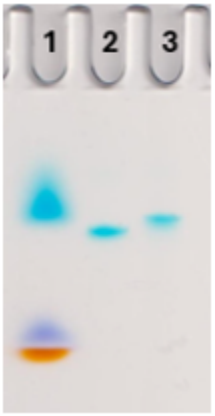

Lane	Contents
1	ULR Ladder
2	5'-DBCO-Cy5-T20-SH-3'
3	5'-HMP-Cy5-T20-SH-3'

Figure 28. PAGE analysis confirms the formation of 5'-HMP-Cy5-T20-SH-3'. Lane 3 shows the expected increase in size for the conjugated product versus the unconjugated oligonucleotide shown in lane 2

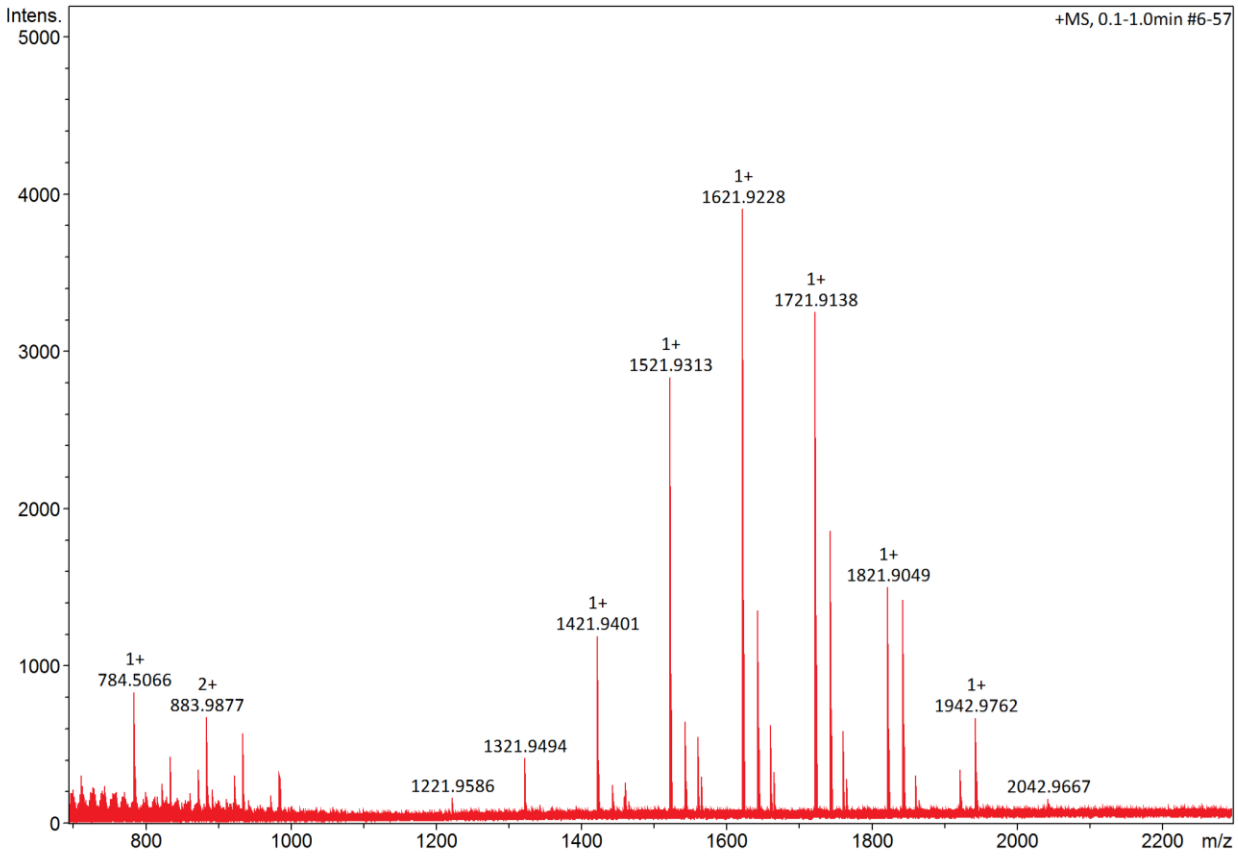

Figure 29. ESI-QTOF analysis of 5'-HMP-Cy5-T20-SH-3'. Found: $[M+6H]^{6+}$ = 1321.9494 , M = 7931.6964 Da, Expected: M = 7924.68 Da

2.5 Functionalization of 5'-HMP-Cy5-T20-SH-3' into spherical nucleic acids

5'-HMP-Cy5-T20-SH-3' which was conjugated at McMaster University was used to form SNAs. The concentration of 5'-HMP-Cy5-T20-SH-3' oligonucleotides and 13 nm gold nanoparticle concentrations were measured by monitoring with a spectrophotometer the absorbance at 260 nm and extinction at 520 nm respectively. 5'-HMP-Cy5-T20-SH-3' oligonucleotides were functionalized onto 13nm gold nanoparticles using a salt-aging process developed in the Mirkin group. [73] DNA loading on the gold nanoparticles was characterized using OliGreen fluorescence assays. This assay depends on OliGreen, a sensitive nucleic acid dye capable of quantifying oligonucleotides and single stranded DNA in solution.[74] In this assay, a calibration curve was made from a two-fold serial dilution of 5'-HMP-Cy5-T20-SH-3' and 5'-T20-SH-3' that were then mixed with OliGreen dye (Figure 30). Triplicate samples of the SNAs at known concentrations of gold were then dissolved in potassium cyanide to release free oligonucleotides, which were also mixed with OliGreen. All samples are then analyzed using a plate reader (excitation 480 nm/emission 520 nm). The fluorescence data from the serial dilution was used make a calibration curve. The fluorescence signals for the SNA samples are then divided by the slope of the calibration curve, which yields the concentration of the oligonucleotides according to Beer's law. The determined DNA concentrations are then divided by the initial concentration of gold nanoparticles to determine the number of DNA strands per gold nanoparticle.

In this SNA synthesis, T20 strand loading was accomplished followed by HMP-Cy5-T20 loading. The calibration curves produced from the assay were used to determine that 232 strands of T20 per gold nanoparticle (Figure 30) and 189 strands of HMP-Cy5-T20 per gold nanoparticle (Figure 31) had been loaded. Using OliGreen assays provided a method to prove and quantify the

level of DNA loading onto gold nanoparticles.[Error! Reference source not found.] Through the assays it was determined that HMP-Cy5-T20 was successfully functionalized onto gold nanoparticles forming the novel target molecule **4**.

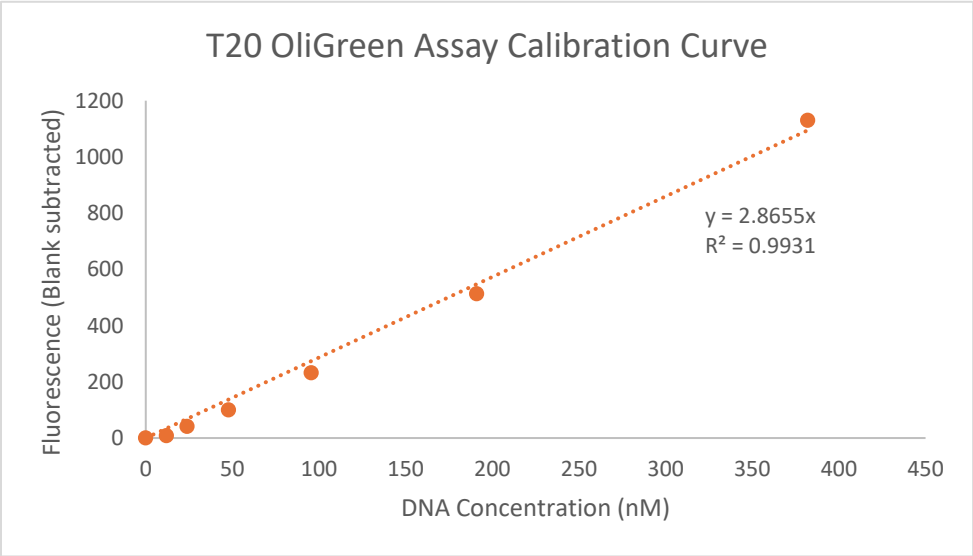

Figure 30. Calibration curve for T20. Excitation (480nm), Emission(520nm)

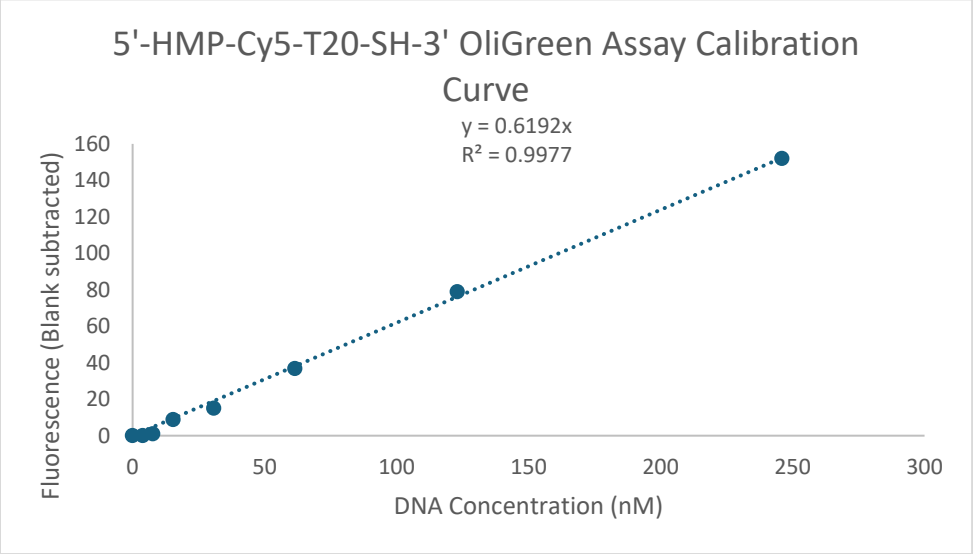

Figure 31. Calibration curve for HMP-Cy5-T20. Excitation (480nm), Emission (520nm)

Chapter 3: Future Directions

This project had the aim of improving cell uptake of heptose phosphates by using SNAs as a nanoscale delivery agent. In this work a bulk synthesis of compound **1** was accomplished. It was then conjugated with a NHS ester PEG4 azide linker, producing compound **2**. In collaboration with the Bujold group, conjugation of **2** with 5'-DBCO-Cy5-T20-SH-3' was successful and produced molecule **3**. SNA synthesis was performed and yielded HMP-functionalized SNAs (molecule **4**). This is the first time that this molecule has been synthesized. This synthesis demonstrates that the functionalization of SNAs with a carbohydrate is possible. With this accomplishment this opens the avenue to further studies of HMP in the cells. SNAs are modular and can have fluorescent dyes added to the strand. With this dye, the activity of HMP can be directly monitored. This would make it possible to visualize the interactions it has as it enters the cell.

One direction that can be taken is to further study the synthesis of HMP-functionalized SNAs. This would require performing and fine-tuning functionalization work to achieve controlled and consistent loading of 5'-HMP-Cy5-T20-SH-3' onto gold nanoparticles. If it is not feasible to sufficiently control the loading of HMP-Cy5-T20 could be measured by level of biological activity. This would lay the groundwork in controlling dosage for this type of molecule.

A worthwhile approach would be further modifying SNAs, to include modified phosphate backbones that are positively charged to varying degrees. In this effort the goal would be increase the level of cell uptake. This avenue would show how well an SNA can be absorbed into cells. The level of cell uptake would be assessed using fluorescence (Cy5 dye) and a flow cytometer.

If the functionalization process can be tuned such that the dosage or concentration of HMP moiety can be controlled, then this molecule would be suitable for testing in Jurkat T cells. The motivation of this work would be to assess its ability to activate IL-8 production in this cell line.[75] The next step would be achieving controlled production of IL-8 such that levels of expression can be reliably attained. In the case that this is made possible, further biological studies can be performed to determine if it would be a suitable latency reversal agent in more complex biological settings such as humanized BLT mice.[9,76]

Chapter 4: Experimental Methods

4.1 Instrumentation

Nuclear magnetic resonance (NMR) spectroscopy was performed using a Varian (^{1}H, 500 MHz, ^{13}C, 125 MHz), Bruker (^{1}H, 600 MHz, ^{13}C, 150 MHz, ^{31}P, 242 MHz), or JEOL (^{1}H, 400 MHz, ^{13}C, 100 MHz) spectrometer with solvent residual signals ($CDCl_3$, 7.26 ppm for ^{1}H, and 77.36 ppm for ^{13}C, and D_2O, 4.79ppm for ^{1}H). The resulting data was interpreted using Delta 6.1.0 and TopSpin 4.1.4 software. Mass spectrometry (MS) data was collected using a SQ2 Detector 2 from Waters and high-resolution mass spectrometry (HRMS) data was collected using a Waters Acquity I-class ultra-performance liquid chromatography (UPLC) system interfaced to a Q Exactive Hybrid quadrupole Orbitrap mass spectrometer equipped with a heated electrospray ionization source. Matrix-Assisted Laser Desorption Ionization Time-of-Flight Mass Spectrometry (MALDI-TOF MS) was performed using a Bruker MALDI-TOF ultrafleXtreme in positive ion mode. Resulting data was interpreted using Bruker Daltonics flexAnalysis. High-performance liquid chromatography (HPLC) was achieved using an Agilent 1280 infinity series.

4.2 General synthetic methods

All reagents were purchased from Sigma Aldrich, Oakwood chemicals, CombiBlocks, or TCI America. All solvents were purchased from Sigma Aldrich or Fisher Scientific. Carbohydrate reactions were performed under nitrogen or argon atmosphere unless stated otherwise or where water was used.

4.3 DNA strand characterization

4.3.1 Ultraviolet-Visible spectroscopy

Through UV-vis spectroscopy the concentration of oligonucleotides and SNAs was determined by using their maximum absorption bands 260 nm and 520 nm, respectively. Scans were collected from 200 nm to 700 nm. Measurements were conducted on a NanoDrop One/One^{C}. Before every measurement, the device was wiped down with deionized water where necessary. All readings were blanked with deionized water.

4.3.2 *Conjugation of* HMP-LINK to *5'*-DBCO-Cy5-T20-*SH-3'*

5'-DBCO-Cy5-T20-SH-3' (30 nmol, 100 µL) was combined with HMP-LINK (300 nmol, 30 µL) in water, and incubated at 37°C overnight in a thermocycler. The following day, the mixture was desalted with a Sephadex column. The conjugate was purified using 20% denaturing PAGE, excised from the gel, which was crushed and soaked overnight, to transfer the oligonucleotides in water. The sample was concentrated prior to desalting. The conjugate was then reduced with DTT to obtain a thiol at the 3' end, concentrated and desalted prior to analysis via ESI-QTOF, which showed a successful conjugation.(Figure 29)

4.3.3 Analytical polyacrylamide gel electrophoresis

Denaturing polyacrylamide gels were made as described in Chapter 2 using a 10-well comb (0.75 mm width) to set lanes within the gel.[77] Samples were prepared by combining 10 µL of 8 M urea and 5 µL of oligonucleotides, which were injected into wells along with a DNA ladder. Gels were run for 1 hour at 100 V and then stained using StainsAll solution (0.05% (w/v)) in formamide/water (1:1, v/v) for 15 minutes.

4.3.4 MALDI-TOF MS

DNA analysis was performed as previously discussed in the MALDI section of Chapter 2.

4.3.5 HPLC analysis of oligonucleotides

DNA samples were dissolved in 25 µL of deionized water and analyzed using reverse phase HPLC using a Poroshell 120 EC-C18 column using 0.1 M triethylammonium acetate buffer pH 7 (buffer A) and acetonitrile (buffer B).[78] DNA was detected at 260 nm and 280 nm. The samples were eluted using a 20-minute linear gradient (0-100% solvent B) followed by 5 minutes of elution at 100% solvent B.

4.4 Spherical Nucleic Acid Synthesis

4.4.1 Dual-layer SNA synthesis

The oligonucleotides used to make SNAs were 5'-DBCO-Cy5-T20-SH-3' and 5'-T20-SH-3' and were synthesized by the Bujold Lab at McMaster University. 5'-DBCO-Cy5-T20-SH-3' was conjugates with HMP-LINK prior to making SNAs. Citrate-capped 13 nm gold nanoparticles were synthesized and provided by the Bujold group.

SNA synthesis was carried out based on published protocols. [73] First, the concentration of the 13 nm citrate-capped gold nanoparticle (AuNP) stock was assessed by diluting 1:10 in deionized water and measuring extinction from 200 to 800 nm on a UV-Vis spectrometer. Beer's law was used to determine the concentration using the known extinction coefficient for these particles of 2.76×10^8 M^{-1} cm^{-1}. Note that Extinction is used since gold nanoparticles are a colloidal suspension, meaning that it both absorbs and diffracts light. This is not a characteristic that is shared with solutions.

Absorbance scans from 200 nm to 700 were done to determine the concentration of the oligonucleotides using their characteristic absorbance peak at 260 nm, ensuring that absorbances between 0.1 and 0.5 arbitrary units (a.u.) were obtained, performing dilutions when necessary to remain within the accurate reading range of the instrument.

Once DNA and AuNP concentrations were determined, they were combined at an 85:1 ratio at a final concentration of 0.85 μM for DNA and 10 nM for the gold nanoparticles with 0.2% Tween-20 to help prevent aggregation. The oligonucleotide used in this step was 5'-HMP-Cy5-T20-SH-3'. The goal of this step is to synthesize a thin monolayer of DNA on the AuNPs that acts as reporter through the Cy5 fluorophore and drug carrier through the presence of the HMP. The second layer will be added to help achieve high cellular uptake. To achieve this, the following reagents were added in order to an Eppendorf tube: AuNPs, water, DNA, then 10% Tween-20. The SNAs were then left to mix in the dark for 15-20 minutes, then 5 M NaCl solution was added slowly to achieve a salt concentration of 0.05 M. The SNAs were subsequently left to mix overnight in the dark.

The next day the monolayer SNAs were pelleted by centrifuging at 13,000 x *g* for 30 minutes. The supernatant was removed, and the pellet was resuspended using Milli-Q water. The centrifugation process was repeated three times to remove excess DNA, surfactant, and salt. On the last centrifugation, water was not added to keep the sample concentrated. Instead, an extinction scan from 200 to 700 nm was performed on the sample, ensuring that extinction remained between 0.1 and 0.5 a.u. through dilution. The extinction at 520 nm and dilution factor were recorded. The volume of the remaining monolayer SNA was determined to determine the number of moles of monolayer SNA present in the sample. The reading from the absorbance of monolayer DNA at 520 nm, and the dilution factor used were used determine the amount of water, DNA, and Tween-20

needed to install a second layer of DNA on the monolayer SNAs at a ratio of 500:1 DNA:SNA at a final DNA concentration of 5 μM and 10 nM for the SNAs. For the second layer, 5'-T20-SH-3' was used to create a dense layer of DNA on the SNA, which assists with cellular uptake. Reagents were added in the following order: SNA, water, DNA, Tween-20. All reagents were added to the Eppendorf containing the monolayer SNA to avoid product loss. The sample was then left to mix overnight in the dark. Note that either strand can be added first or second, as long as the rest of method

4.4.2 Salt-aging of the dual-layer SNAs

To ensure maximal DNA loading on the SNAs, 5 M NaCl was slowly added to the dual-layer in 20-30-minute intervals and 0.05 M increments until a final concentration of 0.5 M was achieved. After each salt addition, the solution was vortexed for about 10 seconds then placed back on the mixer. Once a concentration of 0.5 M NaCl was achieved, the SNAs were left to mix overnight. On the next day, the dual-layer SNAs were washed and pelleted, aspirating the supernatant and replacing with Milli-Q water.

4.4.3 Quantification of DNA loading using OliGreen assays

OliGreen assays were performed to determine the DNA loading density on the monolayer and dual-layer SNAs. DNA stock solutions at approximately 1 μM concentrations (5'-HMP-Cy5-T20-SH-3' and 5'-T20-SH-3') and SNA stock solutions at approximately 1 nM were prepared and their exact concentrations were assessed using UV-Vis spectroscopy. The SNA samples (160 μL) were incubated with 160 μL of 40 mM KCN to dissolve the AuNPs and release the DNA in solution in a tube labeled "SNA+KCN". Using a 96-well plate, 40 mM KCN was added to well A8 with 100 μL of the oligonucleotide stock solution of interest. In wells A1 to A7, 100 μL of 20 mM KCN was added. A 2X serial dilution was performed starting by transferring 100 μL from A8 to A7 and

continued until A2. This left well A1 as is to act as blank. In wells A9 to A11 100 µL from tube labelled as "SNA+KCN". To enable fluorescent detection of the DNA, 100 µL of 200X diluted OliGreen dye was added to wells A1 to A11. The plate was analyzed within 10 minutes to obtain a fluorescence reading using a plate reader with excitation-emission 480/520. The data from this assay was used to produce a calibration curve from a scatter plot of corrected fluorescence values vs. DNA concentration. Using this calibration curve, the level of DNA loading on the gold nanoparticles could be determined for monolayer and dual-layer SNAs.

4.4.4 Agarose gel electrophoresis

Agarose gels were used to assess the monodispersity and relative size of monolayer and dual-layer SNAs. Gels were cast by combining 0.5 g of agarose with 50 mL of 1X TBE buffer, which was then microwaved in 20 second intervals until agarose was fully dissolved in solution and had become clear. When necessary, additional water was added to bring total volume back to 50 mL, and then the gel was poured into a gel box. A 10-well comb with a width of 0.75 mm was inserted into the gel box as the agarose cooled over 30 minutes at room temperature. Once solidified the gel was placed in 1X TBE buffer, and SNAs were loaded in a concentration of approximately 20 nM with 10% glycerol (v/v). Agarose gels were run for 1 hour at 100 V and 50 mA.

4.5 5'-PEG4-7-*O*-(amidoethyl)-D-glycero-β-D-manno-heptopyranose phosphate-Cy5-T20-SH-3' synthesis

All NMR and MS data for synthesized compounds aligned with published compound data.

Note that compounds 1 and 6 to 18 were synthesized as described in Sauvageau et al. with minor changes.[29]

*4.5.1 2,3,5,6-Di-O-isopropylidene-α-D-mannofuranoside (**6**)*

D-mannose (21 g, 116.6 mmol, **5**) was co-evaporated using anhydrous toluene. Anhydrous acetone (500 mL) was added to D-mannose followed by the addition of $FeCl_3$ (6.3 g, 38.8 mmol). The mixture was left to stir overnight at RT under nitrogen. The following day, the reaction was neutralized using $NaHCO_3$ solution (20% by volume of the reaction mixture). Subsequently, the mixture was concentrated, and extracted using DCM with water, sodium bicarbonate, then brine. Using Na_2SO_4, the organic layer was dried. Na_2SO_4 was filtered out and the organic layer was concentrated until a white powder remained. The powder underwent recrystallization using DCM to yield compound **6** (57%, 66.4 mmol, 17.4 g).

^{1}H NMR, (500 MHz, $CDCl_3$) δ 5.39 ($J_{H1',H2'}$= 1.63Hz, d, 1H, H1`), 4.83 ($J_{H3',H2'}$= 6.1Hz, $J_{H3',H4'}$=3.71Hz, dd, 1H, H3'), 4.63 ($J_{H2',H3'}$=6.28Hz, d, 1H, H2`), 4.42 (m, 1H, H5`), 4.20 ($J_{H4',H3'}$= 3.61Hz, $J_{H4',H5'}$ =7.04Hz, dd, 1H, H4`),4.06 (m, 2H, H6`), 2.38 (s, 1H, OH), 1.47 (3H, s, $CH_3$COCH2`, OCH3`), 1.466 (3H, s, $CH_3$COCH5, OCH6`), 1.39 (3H, s, CH_3COCH5`, OCH6`), 1.34 (3H, s, CH_3COCH2`, OCH3`).^{13}C NMR (125 MHz, $CDCl_3$) δ 112.65 (C2`, 3`O_2C), 109.11 (C5`, 6`O_2C), 101.27 (C1`), 85.52 (C2`), 80.26 (C4`), 79.70 (C3`), 66.52 (C6'), 26.84 (CH3COCH5`,OCH6`), 25.87 (CH3COCH2`,OCH3`), 25.18 (CH3COCH5`,OCH6`), 24.47(CH3COCH2`,OCH3`). LRMS Calc'd for $C_{12}H_{20}O_6$ $[M - OH2 - e-]^{+\bullet}$ = 260.28, found = 262.94) .

4.5.2 4-methoxybenzyl 2,3,5,6-di-O-isoproylidene-α-D-mannofuranoside (7)

The following intermediate was synthesized. Using toluene, **6** was dried, then dissolved in anhydrous DMF. Subsequently it was cooled to 0 °C then sodium hydride (60% in mineral oil,

32.9 g, 1372.9 mmol) was slowly added to the mixture. After 30 minutes *p*-methoxybenzyl chloride (115.4 g, 736.8 mmol) was added dropwise, then left to stir for 1 h. Methanol was added slowly to quench the reaction. An extraction was performed using EtOAc and water. The remaining organic fraction was then dried using Na_2SO_4, filtered, and concentrated. The residue was purified using silica gel chromatography, thus affording compound **7** (107.2 g, 281.3 mmol, 61.5%).

^{1}H NMR, (500 MHz, $CDCl_3$) δ 7.27 ($J_{\underline{CH}CCH2,\ \underline{CH}COMe}$ = 8Hz, d, 2H, $\underline{CH}CCH_2$, PMB), 6.91 ($J_{\underline{CH}COMe,\ \underline{CH}CCH2}$ = 8.5Hz, d, 2H, $\underline{CH}$COMe, PMB), 5.07 (s, 1H, H1'), 4.80 ($J_{H3',H2'}$ = 5.86Hz, $J_{H3',H4'}$ = 4.12Hz, dd, 1H, H3'), 4.65 ($J_{H2',H3'}$ = 6.24Hz, d, 1H, H2'), 4.61 ($J_{CHA,\ CHB}$ = 11.53Hz, ABX, 1H, CHA, PMB), 4.44 (m, 2H, CHB, PMB and H5'), 4.14 ($J_{H6'A,\ H6'B}$ = 8.53Hz, $J_{H6'A,H5'}$ = 6.45Hz, ABX, 1H, H6'A), 4.06 ($J_{H6'B,\ H6'A}$ = 8.84Hz, $J_{H6'B,H5'}$ = 4.51Hz, ABX, 1H, H6'B), 3.99($J_{H4',H3'}$ = 3.66Hz, $J_{H4',H5'}$ = 7.79Hz, dd, 1H, H4'), 3.82 (3H, s, CH_3O), 1.48 (6H, s, $\underline{CH_3}$COCH2`,OCH3` and $\underline{CH_3}$COCH5`,OCH6`), 1.41(3H, s, $\underline{CH_3}$COCH5`,OCH6`), 1.33 (3H, s, $\underline{CH_3}$COCH2`,OCH3`). LRMS Calc'd for $C_{20}H_{28}O_7N$ [M – PMB +NH4]+.= 261.07, found = 260.76.

*4.5.3 4-methoxybenzyl 2,3-O-isopropylidene-α-D-mannofuranoside (**8**)*

In a mixture of acetic acid and water (4:1, v/v) compound **7** (0.013 mol, 5.0 g) was dissolved, and left to stir at RT overnight. The reaction mixture was concentrated using toluene. Purification using column chromatography (EtOAc/Hexanes) provided a yield of 99% (0.013 mol, 4.6 g.) of **8**.

^{1}H NMR, (500 MHz, $CDCl_3$) δ 7.25 ($J_{\underline{CH}CCH2,\ \underline{CH}COMe}$ = 7.9Hz, d, 2H, $\underline{CH}CCH_2$, PMB), 6.88 ($J_{\underline{CH}COMe,\ \underline{CH}CCH2}$ = 10.5Hz, d, 2H, $\underline{CH}$COMe, PMB), 5.09 (s, 1H, H1'), 4.85 ($J_{H3',H2'}$ = 5.92Hz, $J_{H3',H4'}$= 3.91Hz, dd, 1H, H3'), 4.63 ($J_{H2',H3'}$ = 5.93Hz, d, 1H, H2'), 4.57 ($J_{CHA,\ CHB}$ = 11.5Hz,

ABX, 1H, CHA, PMB), 4.43 ($J_{CHB,\ CHA}$ = 12Hz, ABX, 1H, CHB, PMB), 4.02 (m, 1H, H5'), 3.98 ($J_{H4',H3'}$ = 3.79Hz, $J_{H4',H5'}$ = 7.87Hz, dd, 1H, H4'), 3.80 (3H, s, CH_3O), 3.84 (m, 1H, H6'A), 3.72 (m, 1H, H6'B) 1.47 (3H, s, CH_3COCH_2`,$OCH_3$`), 1.32 (3H, s, CH_3COCH2`,OCH3`).

*4.5.4 Methyl [methoxybenzyl (Z)-5,6-dideoxy-2,3-O-isopropylidene-α-D-lyxo-hept-5-enofuranosid]uronate (**10**)*

8 (4.6 g, 13.6 mmol) was dissolved in a solution of ice-cold acetone and water (6:1, v/v) then sodium periodate (4.4 g, 20.4 mmol) was added. The mixture stirred for three hours at 0°C, followed by continued stirring at RT overnight. The following day the mixture was concentrated, dissolved in EtOAc, then filtered. The intermediate **9**, was washed with saturated ammonium chloride, and brine. Subsequently it was dried with Na_2SO_4 then concentrated. Using ice cold anhydrous toluene, the intermediate was dissolved. (Methoxycarbonylmethylene)phosphorane (4.3 g, 14 mmol) was added and the mixture was left to stir for 2h. The mixture was then concentrated and purified using flash column chromatography to afford compound **10** (36%, 10.3 mmol, 3.2 g).

^{1}H NMR, (500 MHz, $CDCl_3$) δ 7.27 ($J_{CHCCH2,\ CHCOMe}$ = 8Hz, d, 2H, $CHCCH_2$, PMB), 6.88 ($J_{CHCOMe,\ CHCCH2}$ = 8.5Hz, d, 2H, CHCOMe, PMB), 6.35 ($J_{H5',H4'}$ = 7.21Hz, $J_{H5',H6'}$ = 11.94Hz, dd, 1H, H5'), 6.01 ($J_{H6',H5'}$ = 11.98Hz, d, 1H, H6'), 5.47 (m, 1H, H4'), 5.11 (s, 1H, H1'), 5.04 ($J_{H3',H2'}$ = 5.34Hz, $J_{H3',H4'}$ = 3.88Hz, dd, 1H, H3'), 4.65 ($J_{H2',H3'}$ = 5.84Hz, d, 1H, H2'), 4.61 ($J_{CHA,\ CHB}$ = 11.28Hz, ABX, 1H, CHA, PMB), 4.46 ($J_{CHB,\ CHA}$ = 11.65Hz, ABX, 1H, CHB, PMB), 3.80 (3H, s, CH_3O, PMB), 3.73 (3H, s, CH_3O, C(O)Me), 1.44 (3H, s, CH_3COCH2`,OCH_3).

*4.5.5 Methoxybenzyl (Z)-5,6-dideoxy-2,3-O-isopropylidene-α-D-lyxo-hept-5-enofuranoside (**11**)*

Compound **10** (26.3 mmol, 9.6 g) was dissolved in dry DCM under N_2. Subsequently, DIBAL (99.8 mmol, 99.8 mL) was injected then the mixture was left to stir for two hours. The reaction was quenched using saturated NH_4Cl and DCM was added resulting in gel formation. The gel underwent filtration over glass wool using DCM then was washed with water. Lastly, compound **11** was obtained in a pure form through column chromatography using hexanes and EtOAc with a 40% yield (10.52 mmol, 3.54 g).

^{1}H NMR, (500 MHz, $CDCl_3$) δ 7.27 ($J_{CHCCH2,\ CHCOMe}$ = 8.15Hz, d, 2H, CHCCH$_2$, PMB), 6.89 ($J_{CHCOMe,\ CHCCH2}$ = 8.4Hz, d, 2H, CHCOMe, PMB), 5.95 (m, 1H, H6'), 5.79 (m, 1H, H5'), 5.09 (s, 1H, H1'), 4.80 (m, 1H, H4'), 4.68 ($J_{H3',H2'}$ = 5.73Hz, $J_{H3',H4'}$ = 3.56Hz, dd, 1H, H3'), 4.65 ($J_{H2',H3'}$ = 6.5Hz, d, 1H, H2'), 4.63 ($J_{CHA,\ CHB}$ = 12Hz, ABX, 1H, CHA, PMB), 4.46 ($J_{CHB,\ CHA}$ = 11.6Hz, ABX, 1H, CHB, PMB), 3.80 (3H, s, CH_3O, PMB), 1.46 (3H, s, CH_3COCH2',OCH3'), 1.30 (3H, s, CH_3COCH2`,OCH_3)

*4.5.6 [Methoxybenzyl-7-O-cyanoethyl-5,6-dideoxy-2,3-O-isopropylidene-α-D-lyxo-(Z)-hept-5-enofuranosid]uronate (**12**)*

Compound **11** (16.6 mmol, 5.6 g) was dissolved in anhydrous acetonitrile, then cooled down to 0°C. Sodium hydride (33.3 mmol, 1.3g) was slowly added in portions to the mixture. After 30 minutes, bromoacetonitrile (25.0 mmol, 1.739 mL) diluted in acetonitrile was added dropwise over one hour and left to stir. After five hours, the reaction is quenched using cool methanol. The solution is warmed to RT and mixed with DCM. Subsequently, it is washed with water, then brine. The organic layer was dried using Na_2SO_4, then compound **12** was purified via flash column chromatography using hexanes and EtOAc to obtain 57% yield (9.6 mmol, 3.6 g).

^{1}H NMR (400 MHz, $CDCl_3$) δ 7.26 (d, *J* = 8.6 Hz, 2H, Ar), 6.87 (d, *J* = 8.7 Hz, 2H, Ar), 5.95 (m, 1H, H5′), 5.81 (m, 1H, H6′), 5.11 (d, *J* = 6Hz 1H, H1′), 4.8 (dd, *J* = 3.6, 7.2 Hz, 1H, H4′), 4.76 (dd, *J* = 3.2, 7.2 Hz, 1H, H3′), 4.69 (d, *J* = 5.6 Hz, 1H, H2′), 4.61 (d, *J* = 11.2 Hz, 1H, OCHAPhOMe), 4.44 (d, *J* = 11.6 Hz, 1H, OCHBPhOMe), 4.25 (m, 2H, H7′A, H7′B), 4.24 (s, 2H, CH2CN), 3.79 (m, 3H, CH3O, PMB), 1.44 (s, 3H, $C(CH_3)_2$), 1.28 (s, 3H, $C(CH_3)_2$)

*4.5.7 Methoxybenzyl-7-O-(cyanoethyl)-2,3-O-isopropylidene-D-glycero-α-D-manno heptofuranoside (**13**)*

Compound **12** (0.1332 mmol, 50 mg) was dissolved in a solution of acetone, dioxane, and water (1:2:1, v:v:v) then was left to stir for 30 minutes at RT. Afterwards OsO_4 (7 mol%, 59 µL, 4% wt. in H_2O) was added and left to stir for 5h. The mixture was diluted with DCM, then ice cold 5M HCl was added. The reaction was quenched using $Na_2S_2O_5$ and water. A separation was performed then the organic layer was concentrated in vacuo. Lastly, compound **13** was purified using flash column chromatography with EtOAc and toluene to provide a yield of 50.79% (0.0646 mmol, 25.4 mg).

^{1}H NMR (600 MHz, $CDCl_3$) δ 7.26 (d, *J* = 8.8 Hz, 2H, Ar), 6.89 (d, *J* = 8.4 Hz, 2H, Ar), 5.12 (s, 1H, H1′), 4.89 (dd, *J* = 5.6, 3.6 Hz, 1H, H3′), 4.64 (d, *J* = 6 Hz, 1H, H2′), 4.60 (d, *J* = 11.6 Hz, 1H, OCHAPhOMe), 4.45 (d, *J* = 11.2 Hz, 1H, OCHBPhOMe), 4.35 (s, 2H, CH_2CN), 4.13 (dd, *J* = 3.6, 6.8 Hz, 1H, H4′), 4.05 (dd, *J* = 6.4 Hz, H5′), 3.98 (m, 1H, H6′), 3.87 (dd, *J* = 2.4, 10 Hz, 1H, H7′A), 3.82−3.78 (m, 4H, CH_3O PMB and H7′B), 1.47 (3H, s, $C(CH_3)_2$), 1.31 (3H, s, $C(CH_3)_2$)

*4.5.8 Methoxybenzyl-7-O-(9-fluorenylmethoxycarbonyl-amidoethyl)-2,3-O-isopropylidene-D-manno Heptofuranoside (**15**)*

Compound **13** was co-evaporated with toluene three times. Subsequently, it was dissolved in tetrahydrofuran, then BMS (0.2584 mmol, 24.5µL) was slowly added. The reaction was set to reflux for 3h at 80°C, then was cooled to 0° C. Methanol was slowly added, then the solution was concentrated. Subsequently, the intermediate (**14**) was dissolved in dioxane and $NaHCO_{3(aq)}$ (1:2 v/v). FmocCl (0.1292 mmol, 0.0334 g) was added to the mixture and left to stir for 16h. The mixture was diluted with water and DCM then a separation using water and DCM was performed. The organic layer was dried with Na_2SO_4, concentrated in vacuo, then purified using flash column chromatography with hexanes and EtOAc to provide a yield of 66.9% (0.03005 mmol, 19.1 mg) and 46.52% over 2 steps of compound **15**.

^{1}H NMR (600 MHz, $CDCl_3$) δ 7.74 (d, J = 6.87 Hz, 2H, Ha, Fmoc), 7.57 (m, 2H, Hb, Fmoc), 7.38 (dd, J = 7.4 Hz, 2H, Hc, Fmoc), 7.30 (m, 2H, Hd, Fmoc), 7.26 (d, J = 9.1 Hz, 2H, Ar), 6.89 (d, J = 8.7 Hz, 2H, Ar), 5.12 (s, 1H, H1′), 4.90 (dd, J = 6, 3.9 Hz, 1H, H3′), 4.64 (d, J = 5.9 Hz, 1H, H2′), 4.58 (d, J = 11.5 Hz, 1H, OCHAPhOMe), 4.45 (d, J = 11.5 Hz, 1H, OCHBPhOMe), 4.35 (s, 2H, CH_2CN), 4.13 (dd, J = 3.7, 7.2 Hz, 1H, H4′), 4.04−3.99 (m, 2H, H5′, H6′), 3.85 (dd, J = 2.5, 10.4 Hz, 1H, H7′A), 3.82−3.78 (m, 4H, CH_3O PMB and H7′B), 1.47 (3H, s, $C(CH_3)_2$), 1.31 (3H, s, $C(CH_3)_2$)

*4.5.9 1,2,3,4,6 – Penta-O-acetyl-7-O-(9-fluorenylmethoxycarbonyl-amidoethyl)- D-glycero D-manno-heptopyranosyl (**16**)*

Compound **15** (2.6 mmol 1.7 g) was dissolved in DCM, and water, then was cooled to 0°C. TFA (7.0 mL) was added to the mixture then it was set to stir for 3h. Subsequently, the reaction mixture was concentrated and coevaporated with toluene six times. Afterwards, anhydrous

pyridine (3.0 mL) and Ac_2O (3.0 mL) was added to the mixture and left to stir for 16h. Following the 16-hour reaction time, the mixture is diluted with DCM, washed twice with $NaHCO_{3\,(sat.\,aq)}$. The organic layer was isolated and dried using Na_2SO_4, concentrated in vacuo, then purified through flash column chromatography using EtOAc and hexanes to afford a yield of 87.81% (2.3 mmol, 1.6 g) of **16**.

^{1}H NMR (600 MHz, $CDCl_3$) δ 7.76 (d, J = 6.87 Hz, 2H, Ha, Fmoc), 7.65 (m, 2H, Hb, Fmoc), 7.41 (dd, J = 7.4 Hz, 2H, Hc, Fmoc), 7.29 (m, 2H, Hd, Fmoc), 6.05 (d, J = 2.0 Hz, 1H, H1′α), 5.82 (br. s, 1H, H1′β), 5.64 (br. s, 1H, NH), 5.50−5.42 (m, 2H, H4′α and H2′β), 5.4 (dd, J = 6 Hz, 1H, H4′β), 5.31 (m, 1H, H3′α), 5.24 (dd, J = 1.6, 1H, H2′α), 5.17−5.01 (m, 3H, H6′α, β and H3′β), 4.42 (dd, J = 7.8, 12.6 Hz, 1H, HfA), 4.34 (dd, J = 5.6, 9.6 Hz, 1H, HfB), 4.24 (m, 1H, Hg), 4.06 (dd, J = 8.9, 1.37 Hz, 1H, H5′α), 3.87−3.71 (m, 2H, H7′A, H5′β), 3.62 (m, 1H, H7′B), 3.53 (m, 2H, CH_2CH_2NH), 3.41 (m, 2H, CH_2NH), 2.24−1.90 (multiplet, 15H, CH3, 19α and 19β)

*4.5.10 Diphenyl (2,3,4,6 – Tetra-O-acetyl-7-O-(9-fluorenylmethoxtcarbonyl-amidoethyl)-D-glycero-β-D-manno-heptopyranosyl) phosphate (**18**)*

Compound **16** (0.5625 mmol, 0.3857 g) was dissolved in DCM, then acetic acid (722µL), and hydrogen bromide in acetic acid (3.61 mL) were added. The reaction was left to stir for 16h. Afterwards the mixture was poured onto ice water, extracted with DCM, and washed with $NaHCO_{3(sat.\,aq)}$ and water. The mixture was concentrated in vacuo then DCM, water, silver triflate (1.125 mmol, 289 mg), and silver carbonate (1.125 mmol, 310 mg) were added and left to mix overnight. Subsequently, the mixture was extracted with water and DCM. The organic layer is dried with Na_2SO_4, filtered, then concentrated in vacuo. The carbohydrate is purified via column chromatography using hexanes and EtOAc to produce a yield of 58% (0.3262 mmol, 208 mg) over

these two initial reactions. The anomeric deprotected carbohydrate (0.3236 mmol, 0.2083 g, **17**) was coevaporated using anhydrous toluene three times, then placed under vacuum overnight. The following morning DPPC (3.236 mmol, 0.671mL) was coevaporated with anhydrous toluene then left under vacuum for 1 hour. The anomeric deprotected carbohydrate was dissolved in anhydrous DCM. DPPC was dissolved in DCM (10 mL) then was added to the carbohydrate solution via syringe pump at rate of 2 mL/hour. The reaction is left to run at RT for 2h under nitrogen. Subsequently, freshly produced TEAB buffer (pH 8) is used to wash the reaction mixture, followed by water, then brine. The organic layer was dried using Na_2SO_4, filtered, then concentrated in vacuo. Flash chromatography was performed with hexanes, DEE, and EtOAc, followed by another round of flash chromatography with DCM and EtOAc to afford a yield of 45.5% (0.1473 mmol, 129 mg) of compound **18**.

^{1}H NMR (600 MHz, $CDCl_3$) δ 7.75 (d, J = 7.33 Hz, 2H, Ha, Fmoc), 7.64 (d, J = 7.56 Hz, 2H, Hb, Fmoc), 7.40−7.23 (m, 10H, Hc and Hd Fmoc and Ar), 7.23− 7.13 (m, 4H, Ar), 5.77 (m, 1H, NH), 5.65 (bs, 1H, H1′), 5.45 (m, 1H, H2′), 5.36 (dd, J = 8.9 Hz, 1H, H4′), 5.16 (m, 1H, H6′), 5.05 (dd, J = 2.8, 8.9 Hz, 1H, H3′), 4.42 (d, J = 7.6, 10.3 Hz, 1H, Hf), 4.21 (d, J = 7.1 Hz, 2H, Hg), 3.90 (dd, J = 4.4 Hz, 8.7 Hz, 1H, H5′), 3.68 (d, J = 4.6, 10.5 Hz, 1H, H7A′), 3.56 (dd, J = 5.5, 10.5 Hz, 1H, H7B′), 3.51 (m, 1H, $CHACH_2NH$), 3.42 (m, 1H, $CHBCH_2NH$), 3.37 (m, 2H, CH_2NH), 2.07, 2.04, 2.02, 1.95 (s, 12H, CH_3)

4.5.11 7-O-(Aminoethyl)-D-glycero-β-D-manno-heptopyranose phosphate (1)

Compound **18** was dissolved in anhydrous methanol under nitrogen, then platinum oxide, PtO_2 (product number 459925). Hydrogen gas is bubbled into the mixture, then the reaction is left to stir. Methanol, $N_{2(g)}$, PtO_2, and $H_{2(g)}$ are replenished daily or more if needed. The reaction is determined to be complete once there was an absence of aromatic signals in ^{1}H NMR (7-7.5ppm).

When the reaction was found to be complete the mixture was filtered through celite, then concentrated via rotary evaporator. The carbohydrate was then dissolved in a mixture of triethylamine, methanol, and water (1:7:2, v/v/v) and left to stir for 16h at RT. The mixture was then concentrated via rotary evaporator then purified using a Bio-Gel P-2 size exclusion column. The carbohydrate (**1**) fractions underwent concentration, and afforded a yield of 80.4% (45 µmol, 15.3 mg).

^{1}H NMR (400 MHz, D2O) δ 5.13 (d, $J_{1,P}$ = 8.7 Hz, 1H, H1′), 4.19 (m, 1H, H6′), 4.03 (d, J = 1.2 Hz, 1H, H2′), 3.90−3.764 (m, 4H, H7′ and $CH_2CH_2NH_2$), 3.71 (dd, J = 3.0, 6.9 Hz, 1H, H3′), 3.5 (dd, J = 6.0 Hz, 1H, H4′), 3.56 (dd, J = 2.3, 6.8 Hz, 1H, H5′), 3.24 (app. t, J = 5.0 Hz, 2H, CH_2NH_2)

*4.5.12 Disodium PEG4 Azide-7-O-(Amidoethyl)-D-glycero-β-D-manno-heptose 1-phosphate (**2**)*

Amine **1** (10mg, 30.1µmol) was dissolved in 500µL of MilliQ water, followed by the addition of Azido-PEG4-NHS ester (13.64mg (90µmol) in 200µL of Dimethylformamide(0.45M)). The mixture was left to stir overnight and then 1 drop of Et_3N was added. After 24h, the reaction was completed (HRMS [M +Na] = 629.2084 *m/z*). The reaction mixture was frozen and lyophilized overnight. The compound was eluted using HPLC (Agilent 1260 Infinity) with MilliQ water and acetonitrile on a C18 column. Using UV light (210nm) and TLC 3.76mg (5.981µmol) of **2** was obtained in a 19% yield as a pale-yellow powder.

^{1}H NMR (600 MHz, D_2O) δ 5.12 (app d, $J_{1,P}$ = 8.75 Hz, 1H, H1′), 4.19 (dt, J=8.38 Hz, 1H, H6′), 4.02 (app s, 1H, H2′), 3.76-3.64 (m, 24H, H3′, H5′, $H7_{a/b}$′, 10 × CH_2), 3.53 (t, J = 5.23 Hz, 2H, H9′, H10′), 3.734 (m, H4′), 3.45 (t, J = 5.4Hz, 2H, C(O)$CH_2C\underline{H_2}$), 2.58 (t, J = 5.65 Hz, 2H, C(O)$C\underline{H_2}$ H11′, H12′) $^{13}C\{^1H\}$ NMR (150 MHz, D_2O) δ 91.15 (C1′), 73.3 (C4′), 66.8 (C2′), 65.33

(CH_2 decyl), 65.33 (CH_2 decyl), 65.33 (CH_2 decyl), 65.33 (CH_2 decyl), 65.33 (CH_2 decyl), 65.33 (CH_2 decyl), 65.33 (CH_2 decyl), 65.33 (CH_2 decyl), 65.33 (CH_2 decyl), 65.3 (C6′), 65.25 (C5′), 64.86 (C7′), 46.08 (C8′), 31.6 (C9′); HRMS *m/z* calc'd for $C_{20}H_{38}N_4O_{15}P$ Na = 604.20, found [M + Na] = 631.2201 .

*4.5.13 Cyanine 5-T20 oligonucleotide-PEG4-7-O-(amidoethyl)-D-glycero-β-D-manno-heptopyranose phosphate (**3**)*

30 nmol of DBCO-Cyanine5-T20 oligonucleotide was mixed with 300nmol of PEG4 Azide-7-O-(Amidoethyl)-D-glycero-β-D-manno-heptose 1-phosphate in deionized water. It was left to mix in a thermocycler overnight. The reaction mixture was then desalted using a 0.2 column Sephadex™ column in a final volume of 400 µL. The mixture was characterized using a 20% analytical denaturing gel (120V, 1h, 0.1 OD per lane). A colorimetric scan, then a StainsAll stain with a scan was performed. **3** was purified via 20% denaturing PAGE (250 V, 45 min, follow up with 500 V, 1.5 h). The bands were heat shocked then extracted overnight at RT. Subsequently recombined with 0.1M DTT in 0.1 M tris pH 8.4, concluded with a concentration and storage are 4°C. ESI-QTOF analysis was done then **3** was sent to National Research Council of Canada (Ottawa) via Xpresspost™.

APPENDIX

A.1 NMR and MS Spectra

^{1}H NMR, **6** (500MHz, $CDCl_3$)

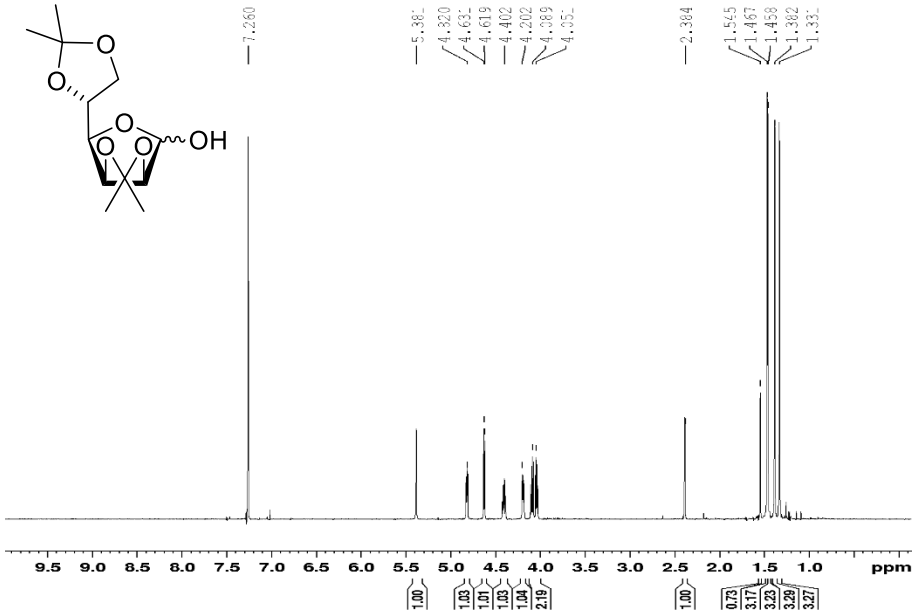

^{13}C{H} NMR, **6** (125MHz, $CDCl_3$)

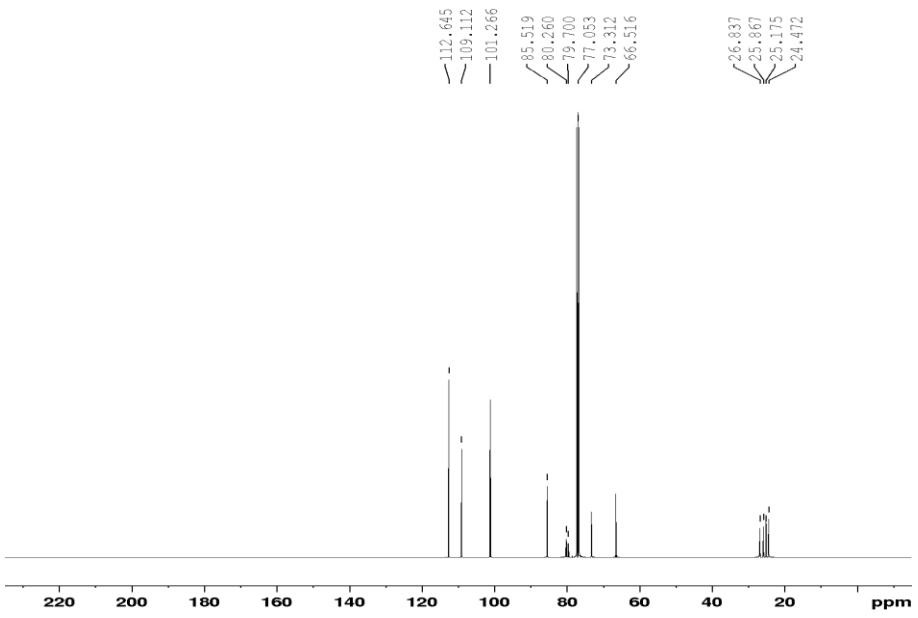

^{1}H NMR, **7** (500MHz, $CDCl_3$)

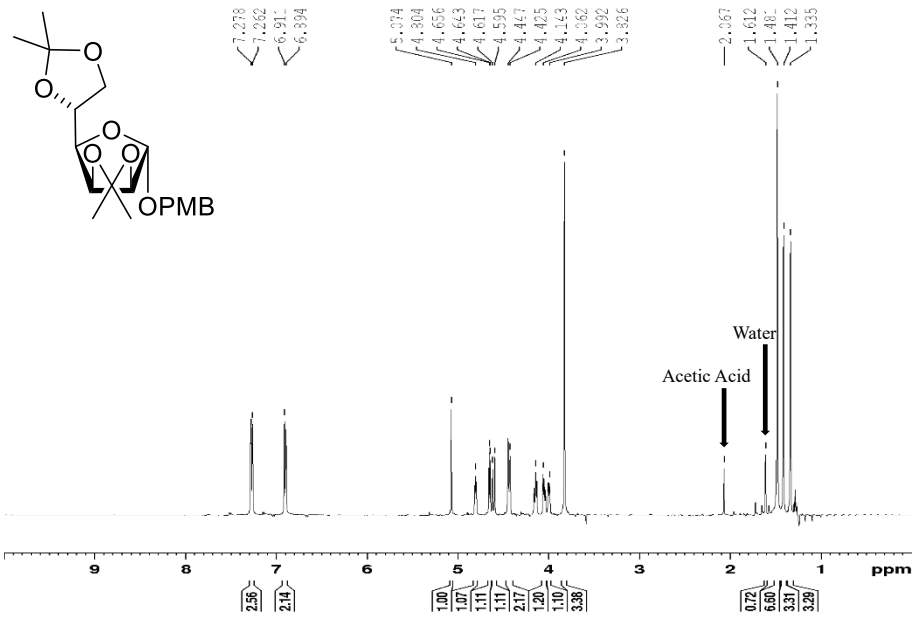

^{1}H NMR, **8** (500MHz, $CDCl_3$)

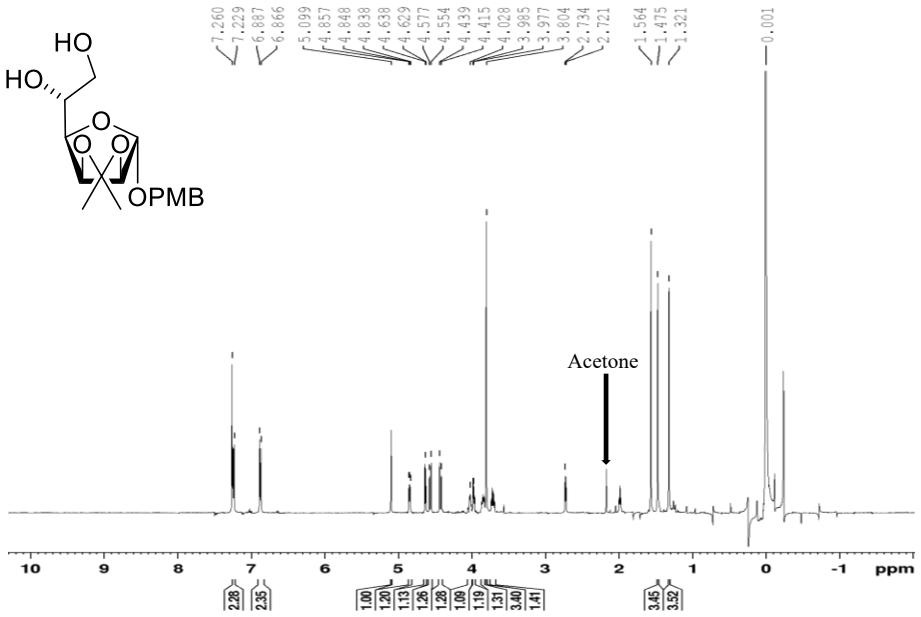

^{1}H NMR, **10** (500MHz, $CDCl_3$)

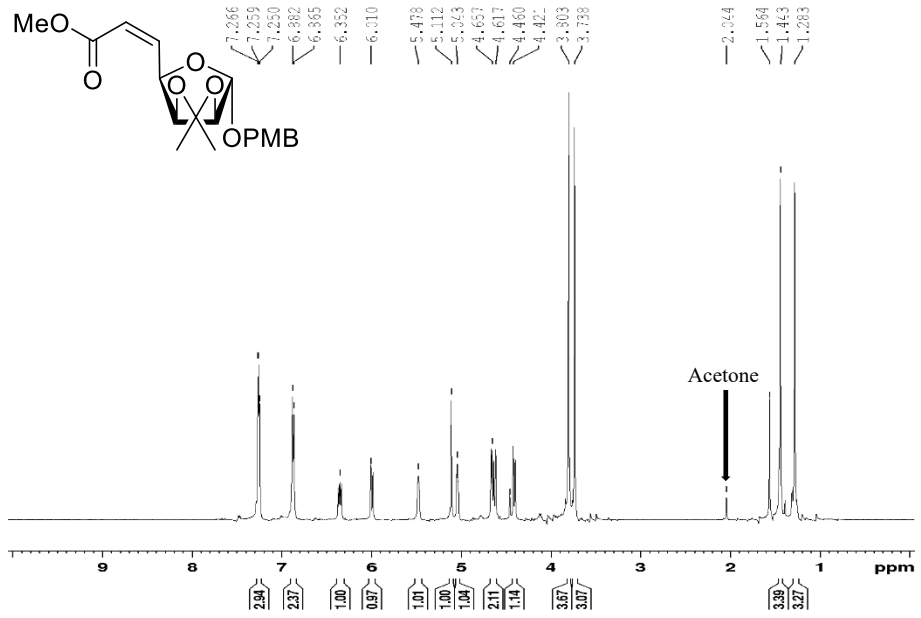

^{1}H NMR, **11** (500MHz, $CDCl_3$)

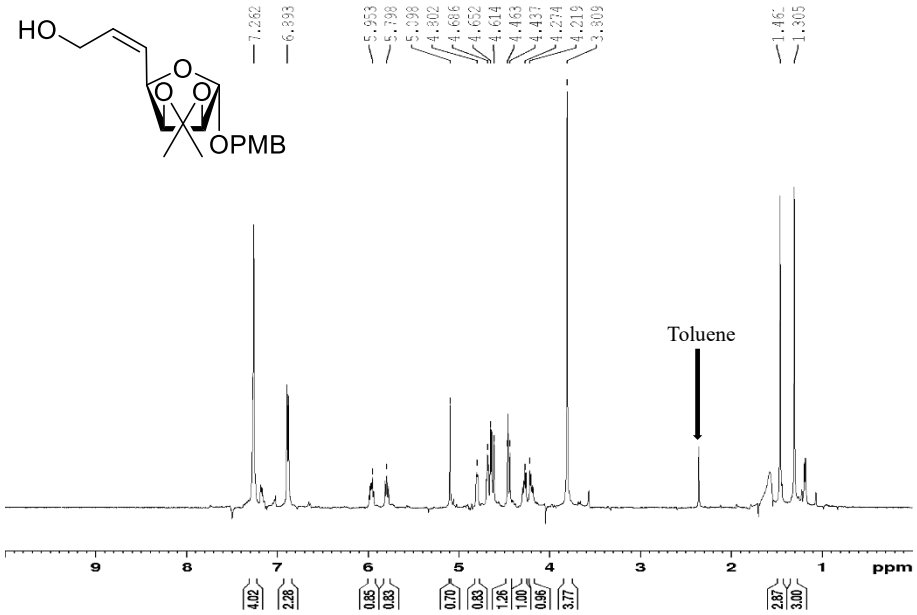

^{1}H NMR, **12** (400MHz, $CDCl_3$)

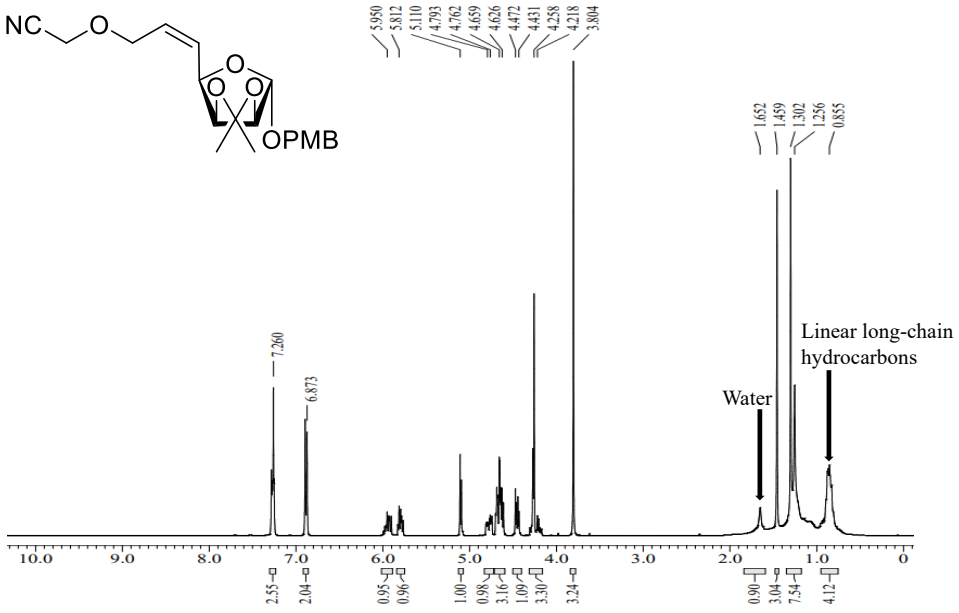

^{1}H NMR, **13** ($CDCl_3$)

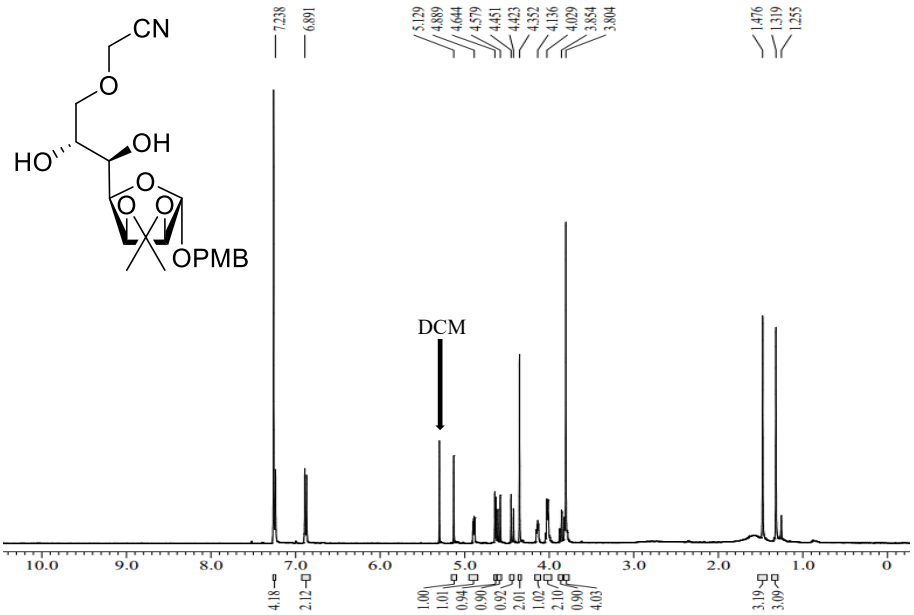

^{1}H NMR, **15** ($CDCl_3$)

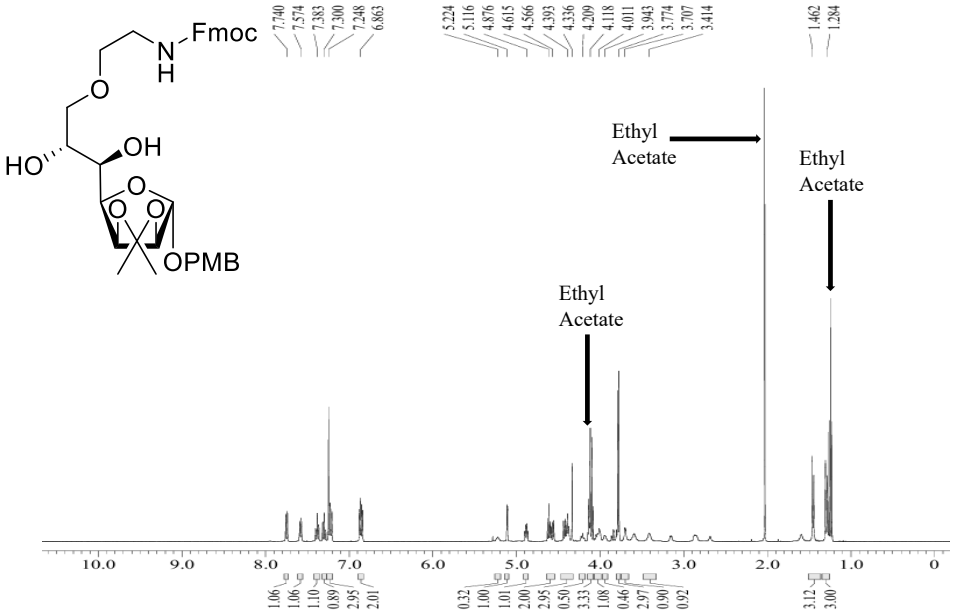

^{1}H NMR, **16** (400MHz, $CDCl_3$)

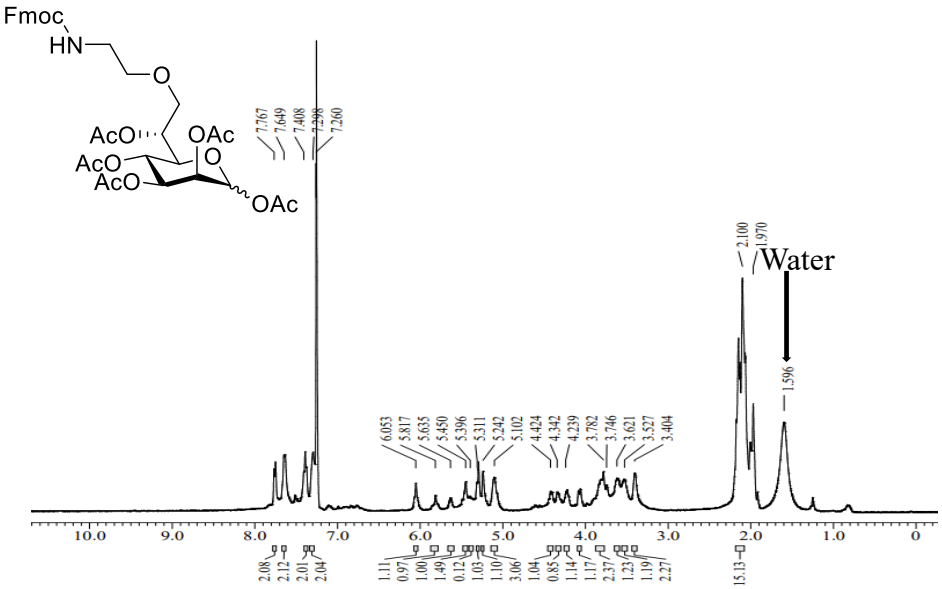

^{1}H NMR, **18** (400MHz, $CDCl_3$)

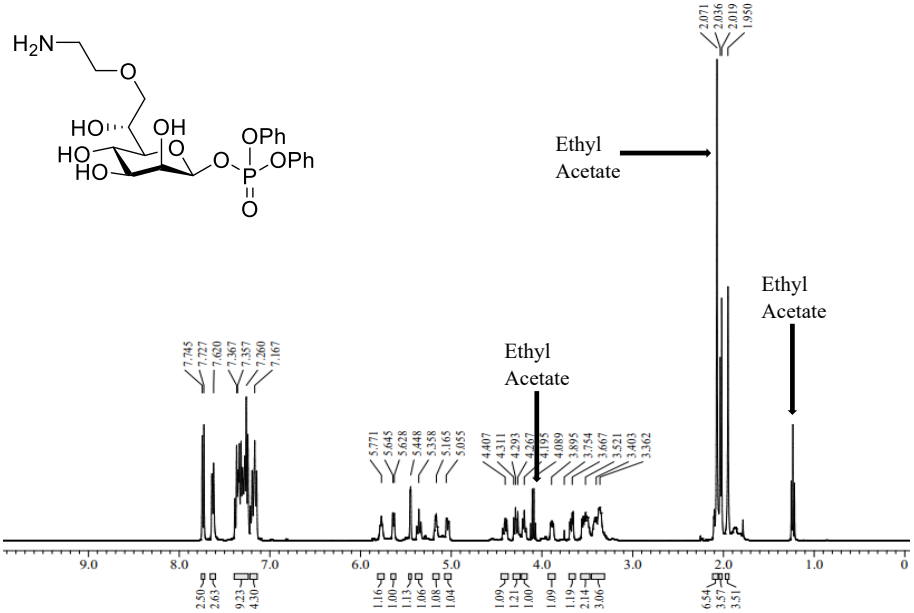

^{1}H NMR, **1** (400MHz, D_2O)

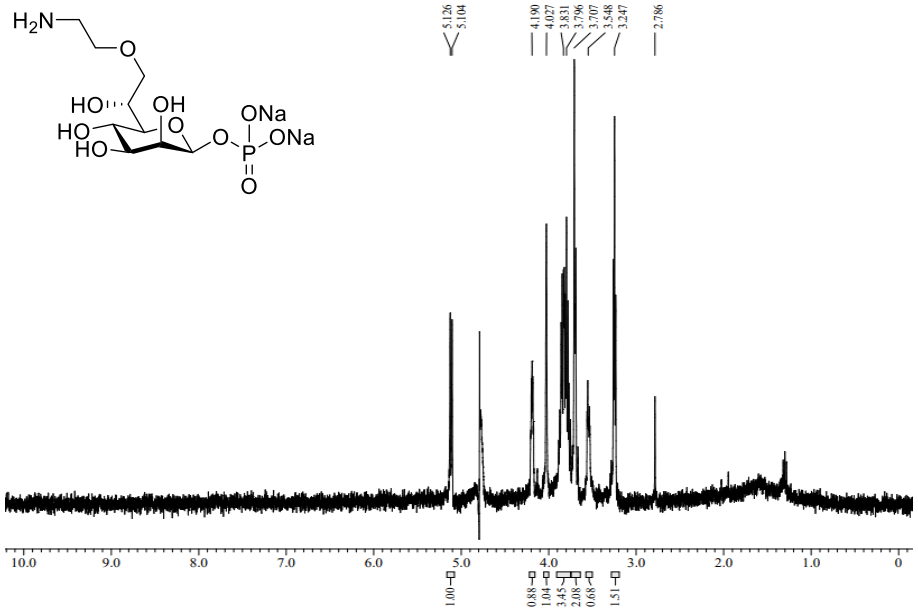

^{1}H NMR, **2** (600MHz, D_2O)

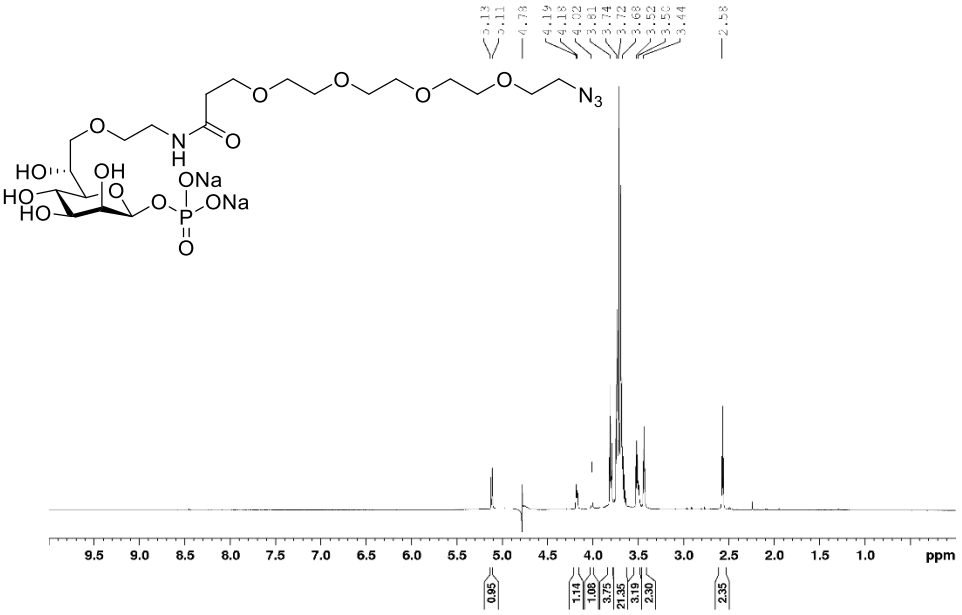

^{13}C NMR, **2** (150MHz, D_2O)

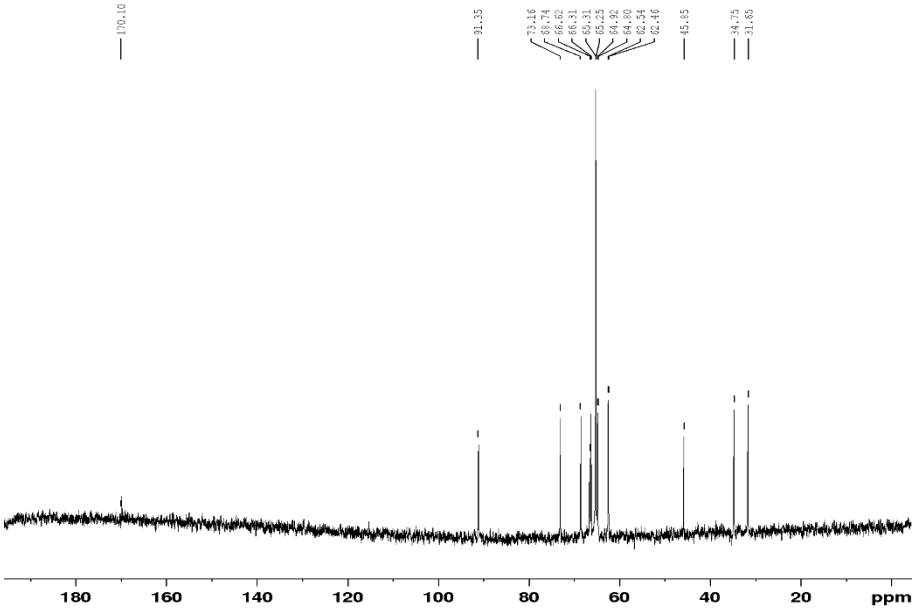

COSY Spectrum, **2** (600 MHz, D_2O)

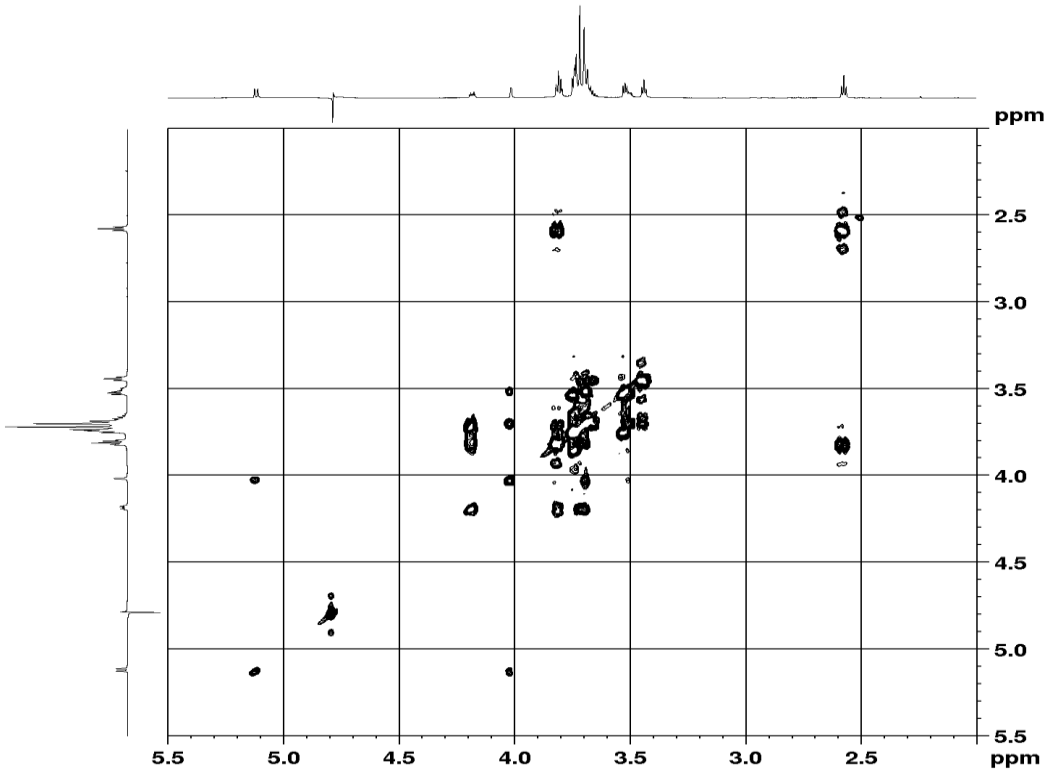

HMBC Spectrum, **2**

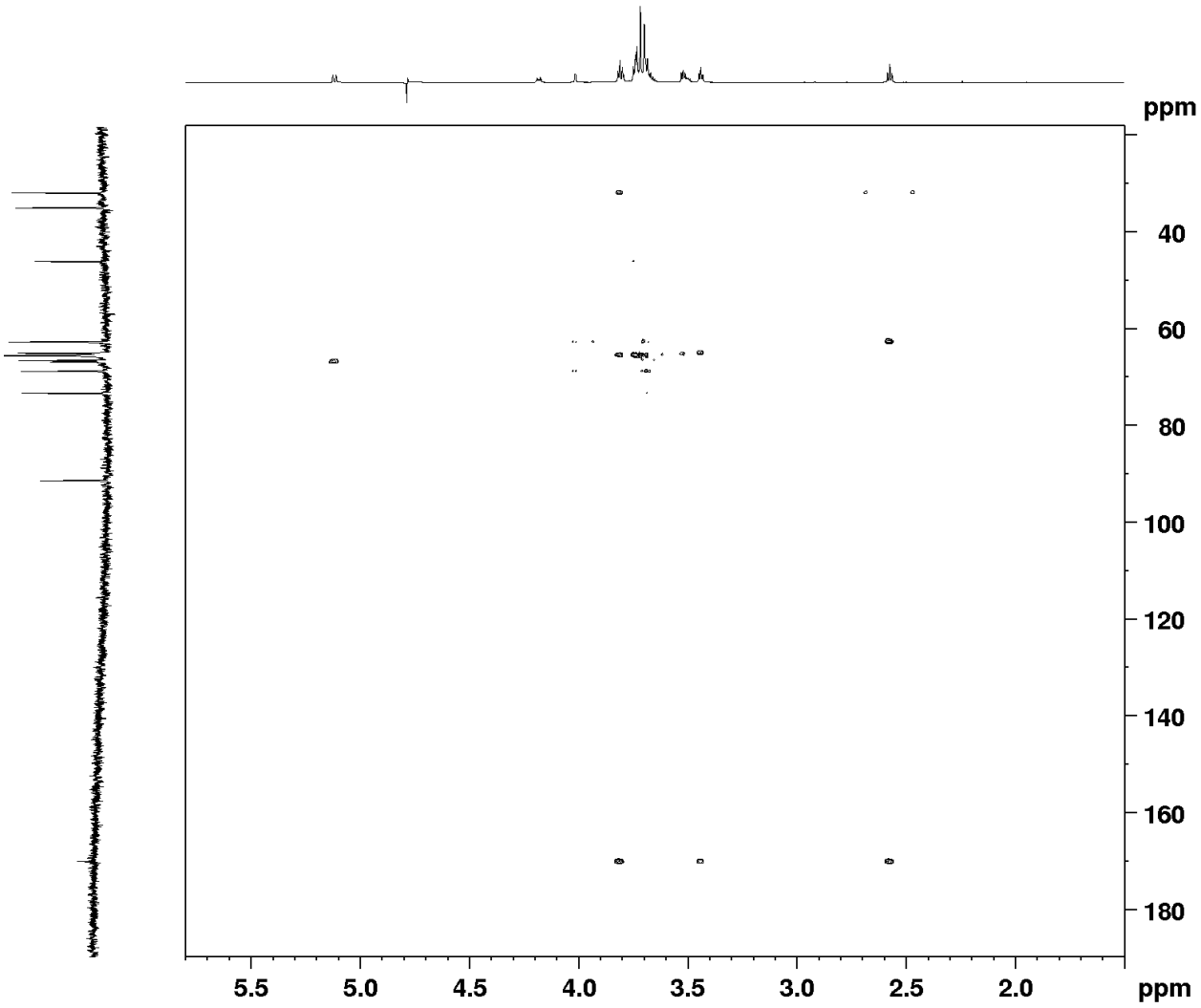

HSQC Spectrum, **2**

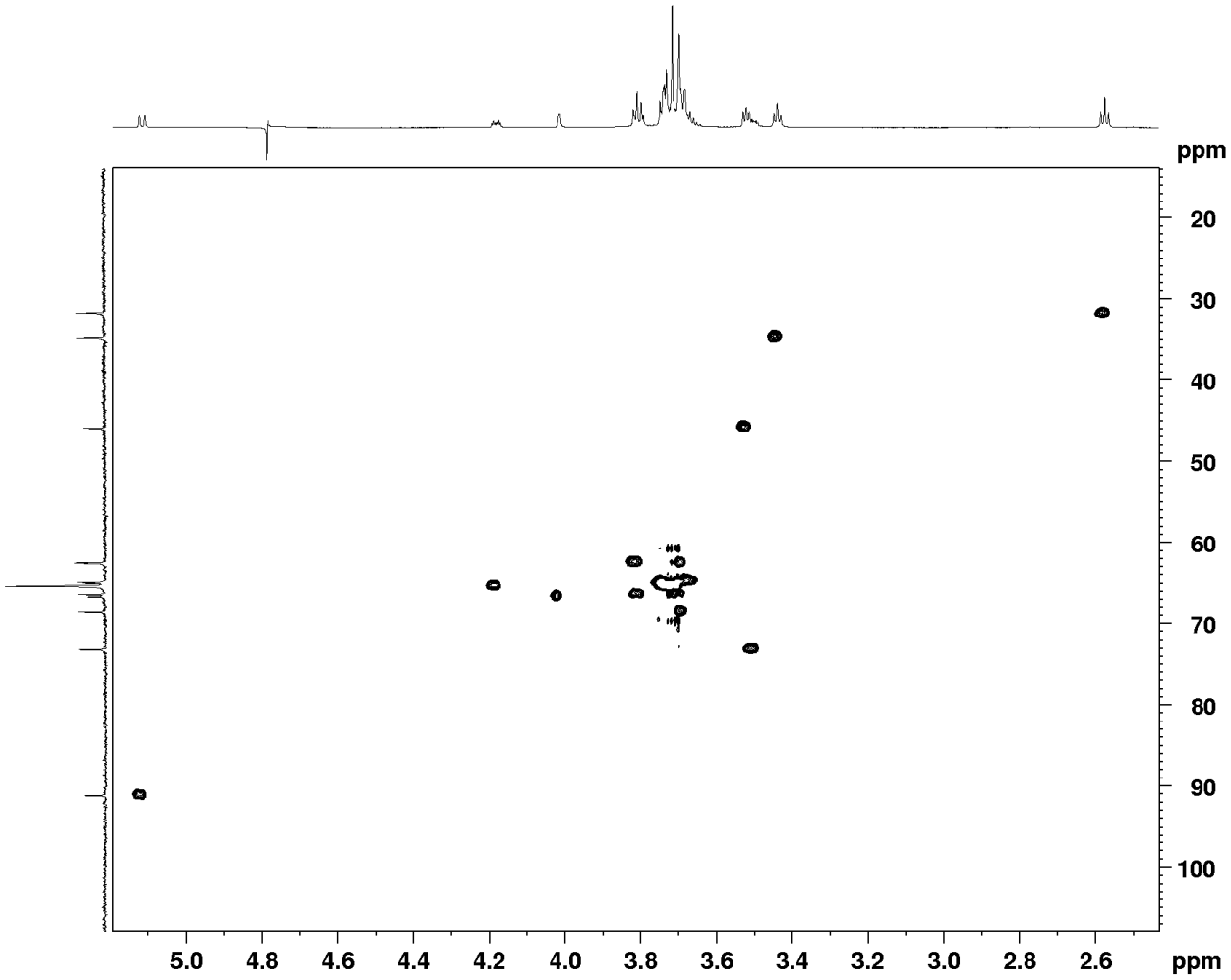

A.2 Assessments of conjugation of HMP-LINK with 5'-DBCO-Cy5-T20-SH-3'

LRMS (ESI) = $C_{50}H_{76}N_6O_{23}P^+$; Calc'd: 1159.47, [M + H] = 1159.8

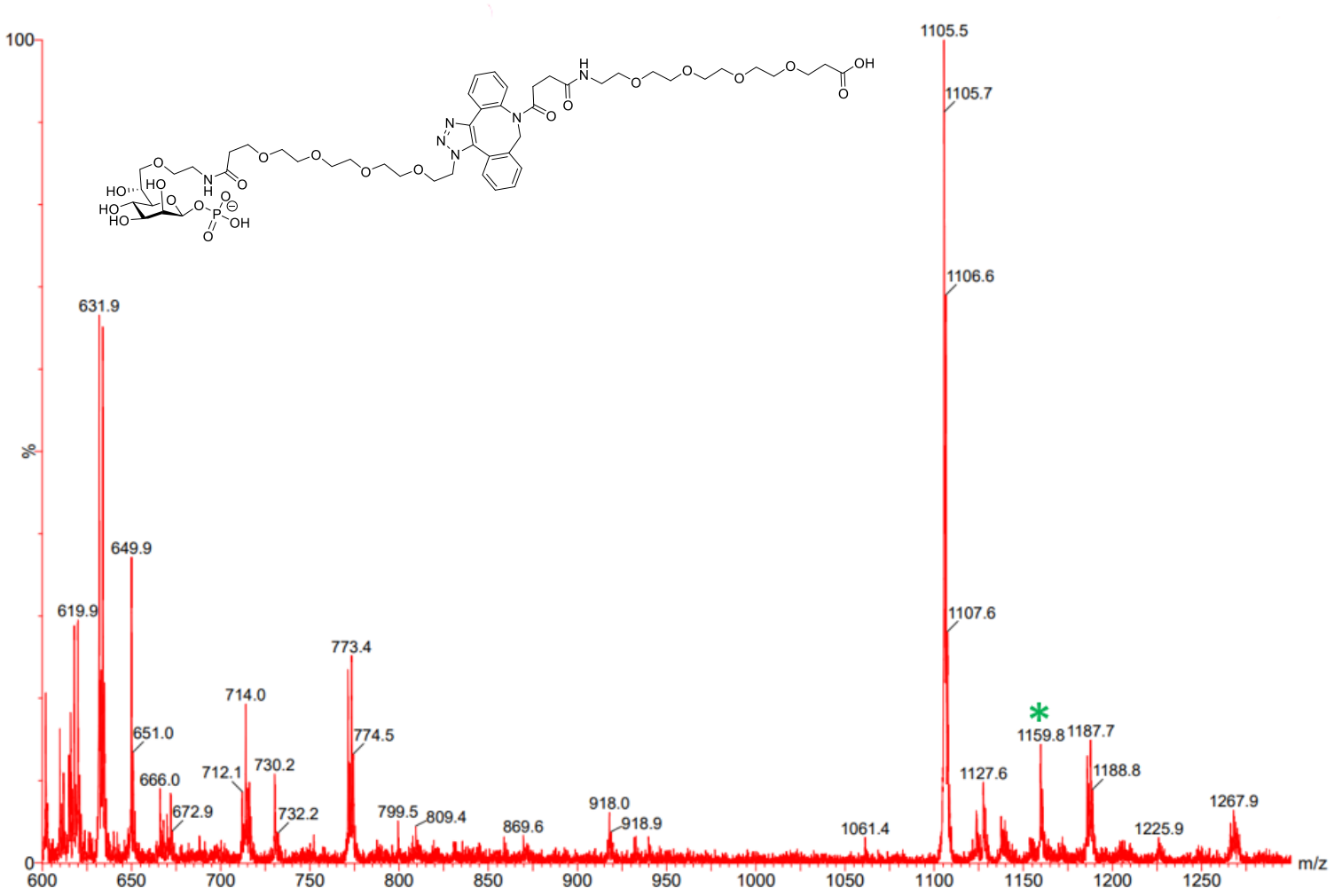

LRMS (ESI)), Calc'd: 605.21, [M + H] = 605.7

HRMS (ESI), $C_{20}H_{39}O_{15}N_4PNa^+$ Calc'd: 629.2042, $[M+Na]^+$ = 629.2084

Bibliography

(1) Adekoya, I. A.; Guo, C. X.; Gray-Owen, S. D.; Cox, A. D.; Sauvageau, J. D-Glycero-β-d-Manno-Heptose 1-Phosphate and d-Glycero-β-d-Manno-Heptose 1,7-Biphosphate Are Both Innate Immune Agonists. *The Journal of Immunology* **2018**, *201* (8), 2385–2391. https://doi.org/10.4049/jimmunol.1801012.

(2) Huang, A.; Pressnall, M. M.; Lu, R.; Huayamares, S. G.; Griffin, J. D.; Groer, C.; DeKosky, B. J.; Forrest, M. L.; Berkland, C. J. Human Intratumoral Therapy: Linking Drug Properties and Tumor Transport of Drugs in Clinical Trials. *Journal of Controlled Release* **2020**, *326*, 203–221. https://doi.org/10.1016/J.JCONREL.2020.06.029.

(3) Bharate, S. B.; Lindsley, C. W. Call for Papers: Natural Products Driven Medicinal Chemistry. *J Med Chem* **2023**, *66* (24), 16455–16456. https://doi.org/10.1021/acs.jmedchem.3c02193.

(4) Batista-Duharte, A.; Lindblad, E. B.; Oviedo-Orta, E. Progress in Understanding Adjuvant Immunotoxicity Mechanisms. *Toxicol Lett* **2011**, *203* (2), 97–105. https://doi.org/10.1016/J.TOXLET.2011.03.001.

(5) van Duin, D.; Medzhitov, R.; Shaw, A. C. Triggering TLR Signaling in Vaccination. *Trends Immunol* **2006**, *27* (1), 49–55. https://doi.org/10.1016/j.it.2005.11.005.

(6) Klinman, D. M.; Currie, D.; Gursel, I.; Verthelyi, D. Use of CpG Oligodeoxynucleotides as Immune Adjuvants. *Immunol Rev* **2004**, *199* (1), 201–216. https://doi.org/https://doi.org/10.1111/j.0105-2896.2004.00148.x.

(7) Yan, Y.; Yao, D.; Li, X. Immunological Mechanism and Clinical Application of PAMP Adjuvants. *Recent Patents on Anti-Cancer Drug Discovery*. 2021, pp 30–43. https://doi.org/http://dx.doi.org/10.2174/1574892816666210201114712.

(8) Malott, R. J.; Keller, B. O.; Gaudet, R. G.; McCaw, S. E.; Lai, C. C. L.; Dobson-Belaire, W. N.; Hobbs, J. L.; St. Michael, F.; Cox, A. D.; Moraes, T. F.; Gray-Owen, S. D. Neisseria Gonorrhoeae-Derived Heptose Elicits an Innate Immune Response and Drives HIV-1 Expression. *Proceedings of the National Academy of Sciences* **2013**, *110* (25), 10234–10239. https://doi.org/10.1073/pnas.1303738110.

(9) Tanaka, K.; Kim, Y.; Roche, M.; Lewin, S. R. The Role of Latency Reversal in HIV Cure Strategies. *J Med Primatol* **2022**, *51* (5), 278–283. https://doi.org/https://doi.org/10.1111/jmp.12613.

(10) Waldman, A. D.; Fritz, J. M.; Lenardo, M. J. A Guide to Cancer Immunotherapy: From T Cell Basic Science to Clinical Practice. *Nat Rev Immunol* **2020**, *20* (11), 651–668. https://doi.org/10.1038/s41577-020-0306-5.

(11) *HIV/AIDS*. https://www.who.int/en/news-room/fact-sheets/detail/hiv-aids (accessed 2020-11-30).

(12) Arts, E. J.; Hazuda, D. J. HIV-1 Antiretroviral Drug Therapy. *Cold Spring Harb Perspect Med* **2012**, *2* (4), a007161. https://doi.org/10.1101/CSHPERSPECT.A007161.

(13) Baynes, H. W.; Tegene, B.; Gebremichael, M.; Birhane, G.; Kedir, W.; Biadgo, B. Assessment of the Effect of Antiretroviral Therapy on Renal and Liver Functions among HIV-Infected Patients: A Retrospective Study. *HIV/AIDS - Research and Palliative Care* **2016**, *9*, 1–7. https://doi.org/10.2147/HIV.S120979.

(14) Finzi, D.; Blankson, J.; Siliciano, J. D.; Margolick, J. B.; Chadwick, K.; Pierson, T.; Smith, K.; Lisziewicz, J.; Lori, F.; Flexner, C.; Quinn, T. C.; Chaisson, R. E.; Rosenberg, E.; Walker, B.; Gange, S.; Gallant, J.; Siliciano, R. F. Latent Infection of CD4+ T Cells Provides a Mechanism for Lifelong Persistence of HIV-1, Even in Patients on Effective Combination Therapy. *Nat Med* **1999**, *5* (5), 512–517. https://doi.org/10.1038/8394.

(15) Li, J. Z.; Aga, E.; Bosch, R. J.; Pilkinton, M.; Kroon, E.; MacLaren, L.; Keefer, M.; Fox, L.; Barr, L.; Acosta, E.; Ananworanich, J.; Coombs, R.; Mellors, J. W.; Landay, A. L.; Macatangay, B.; Deeks, S.; Gandhi, R. T.; Smith, D. M.; Team, A. C. T. G. A. S. Time to Viral Rebound After Interruption of Modern Antiretroviral Therapies. *Clinical Infectious Diseases* **2022**, *74* (5), 865–870. https://doi.org/10.1093/cid/ciab541.

(16) Kim, Y.; Anderson, J. L.; Lewin, S. R. Getting the "Kill" into "Shock and Kill": Strategies to Eliminate Latent HIV. *Cell Host Microbe* **2018**, *23* (1), 14–26. https://doi.org/10.1016/j.chom.2017.12.004.

(17) Fiume, G.; Vecchio, E.; De Laurentiis, A.; Trimboli, F.; Palmieri, C.; Pisano, A.; Falcone, C.; Pontoriero, M.; Rossi, A.; Scialdone, A.; Fasanella Masci, F.; Scala, G.; Quinto, I. Human Immunodeficiency Virus-1 Tat Activates NF-KB via Physical Interaction with IκB-α and P65. *Nucleic Acids Res* **2012**, *40* (8), 3548–3562. https://doi.org/10.1093/nar/gkr1224.

(18) Cox, A.; Gray-Owen, S.; Sauvageau, J.; Guo, X. D-GLYCERO-B-D-HEPTOSE 1-PHOSPHATE (HMP) CONJUGATES AND USE FOR TARGETED IMMUNE MODULATION. https://www.ic.gc.ca/opic-cipo/cpd/eng/patent/3086690/summary.html?type=number_search&tabs1Index=tabs1_1.

(19) *US12036229B2 - Use of phosphorylated heptose compounds - Google Patents*. https://patents.google.com/patent/US12036229B2/fr (accessed 2024-12-01).

(20) Gaudet, R. G.; Sintsova, A.; Buckwalter, C. M.; Leung, N.; Cochrane, A.; Li, J.; Cox, A. D.; Moffat, J.; Gray-Owen, S. D. Cytosolic Detection of the Bacterial Metabolite HBP Activates TIFA-Dependent Innate Immunity. *Science (1979)* **2015**, *348* (6240), 1251–1255. https://doi.org/10.1126/SCIENCE.AAA4921/SUPPL_FILE/GAUDET.SM.PDF.

(21) McNaught, A. D. Nomenclature of Carbohydrates (IUPAC Recommendations 1996). **1996**, *68* (10), 1919–2008. https://doi.org/doi:10.1351/pac199668101919.

(22) Inuki, S.; Aiba, T.; Kawakami, S.; Akiyama, T.; Inoue, J.; Fujimoto, Y. Chemical Synthesis of D-Glycero-d-Manno-Heptose 1,7-Bisphosphate and Evaluation of Its Ability to

Modulate NF-KB Activation. *Org Lett* **2017**, *19* (12), 3079–3082. https://doi.org/10.1021/acs.orglett.7b01158.

(23) Williams, D.; Williams Mohammad Jamshidi, D. P.; Sauvageau, J.; Oh Ho Ho Oh O R, O. H.; Ho R, O. H. Pathogen-Associated Molecular Patterns: The Synthesis of Heptose Phosphates and Derivatives. *Synthesis (Stuttg)* **2022**, *54* (01), 79–91. https://doi.org/10.1055/S-0040-1720179.

(24) Liang, L.; Cao, J.; Wei, T.-Y. W.; Tsai, M.-D.; Vincent, S. P. Synthesis of a Biotinylated Heptose 1,7-Bisphosphate Analogue, a Probe to Study Immunity and Inflammation. *Org Biomol Chem* **2021**, *19* (22), 4943–4948. https://doi.org/10.1039/D1OB00790D.

(25) Lewbart, M. L.; Schneider, J. J. Preparation and Properties of Steroidal 17,20- and 20,21-Acetonides Epimeric at C-20. I. Derivatives of 5.Beta.-Pregnan-3.Alpha.-Ol. *J Org Chem* **1969**, *34* (11), 3505–3512. https://doi.org/10.1021/jo01263a062.

(26) Marco, J. L.; Hueso-Rodríguez, J. A. Synthesis of Optically Pure 1-(3-Furyl)-1,2-Dihydroxyethane Derivatives. *Tetrahedron Lett* **1988**, *29* (20), 2459–2462. https://doi.org/10.1016/S0040-4039(00)87907-1.

(27) Brimacombe, J. S.; Kabir, A. K. M. S. The Synthesis of Some Seven-Carbon Sugars via the Osmylation of Olefinic Sugars. *Carbohydr Res* **1986**, *150* (1), 35–51. https://doi.org/10.1016/0008-6215(86)80004-0.

(28) Schroeder, M. Osmium Tetraoxide Cis Hydroxylation of Unsaturated Substrates. *Chem Rev* **1980**, *80* (2), 187–213. https://doi.org/10.1021/cr60324a003.

(29) Sauvageau, J.; Bhasin, M.; Guo, C. X.; Adekoya, I. A.; Gray-Owen, S. D.; Oscarson, S.; Guazzelli, L.; Cox, A. Alternate Synthesis to D-Glycero-β-d-Manno-Heptose 1,7-Biphosphate. *Carbohydr Res* **2017**, *450*, 38–43. https://doi.org/10.1016/J.CARRES.2017.08.011.

(30) Moss, G. P. Basic Terminology of Stereochemistry (IUPAC Recommendations 1996). **1996**, *68* (12), 2193–2222. https://doi.org/doi:10.1351/pac199668122193.

(31) Tvaroŝka, I.; Bleha, T. Anomeric and Exo-Anomeric Effects in Carbohydrate Chemistry. *Adv Carbohydr Chem Biochem* **1989**, *47* (C), 45–123. https://doi.org/10.1016/S0065-2318(08)60412-6.

(32) Garegg, P. J. Saccharides of Biological Importance: Challenges and Opportunities for Organic Synthesis. *Acc Chem Res* **1992**, *25* (12), 575–580. https://doi.org/10.1021/ar00024a005.

(33) Borio, A.; Hofinger, A.; Kosma, P.; Zamyatina, A. Chemical Synthesis of the Innate Immune Modulator – Bacterial d-Glycero-β-d-Manno-Heptose-1,7-Bisphosphate (HBP). *Tetrahedron Lett* **2017**, *58* (29), 2826–2829. https://doi.org/10.1016/J.TETLET.2017.06.014.

(34) Milivojevic, M.; Dangeard, A.-S.; Kasper, C. A.; Tschon, T.; Emmenlauer, M.; Pique, C.; Schnupf, P.; Guignot, J.; Arrieumerlou, C. ALPK1 Controls TIFA/TRAF6-Dependent Innate Immunity against Heptose-1,7-Bisphosphate of Gram-Negative Bacteria. *PLoS Pathog* **2017**, *13* (2), e1006224.

(35) Zhang, R.; Qin, X.; Kong, F.; Chen, P.; Pan, G. Improving Cellular Uptake of Therapeutic Entities through Interaction with Components of Cell Membrane. *Drug Deliv* **2019**, *26* (1), 328–342. https://doi.org/10.1080/10717544.2019.1582730.

(36) Lipinski, C. A. Lead- and Drug-like Compounds: The Rule-of-Five Revolution. *Drug Discov Today Technol* **2004**, *1* (4), 337–341. https://doi.org/10.1016/J.DDTEC.2004.11.007.

(37) Rautio, J.; Meanwell, N. A.; Di, L.; Hageman, M. J. The Expanding Role of Prodrugs in Contemporary Drug Design and Development. *Nat Rev Drug Discov* **2018**, *17* (8), 559–587. https://doi.org/10.1038/nrd.2018.46.

(38) Liu, P.; Chen, G.; Zhang, J. A Review of Liposomes as a Drug Delivery System: Current Status of Approved Products, Regulatory Environments, and Future Perspectives. *Molecules*. 2022. https://doi.org/10.3390/molecules27041372.

(39) Li, T.; Tikad, A.; Pan, W.; Vincent, S. P. β-Stereoselective Phosphorylations Applied to the Synthesis of ADP- and Polyprenyl-β-Mannopyranosides. *Org Lett* **2014**, *16* (21), 5628–5631. https://doi.org/10.1021/ol5026876.

(40) Calderón, C.; Lämmerhofer, M. Basic Principles for the Selection of Liquid Chromatographic Modes for Specific Applications. *Liquid Chromatography: Applications* **2023**, 81–157. https://doi.org/10.1016/B978-0-323-99969-4.00101-7.

(41) Pfannkuch, L.; Hurwitz, R.; Trauisen, J.; Sigulla, J.; Poeschke, M.; Matzner, L.; Kosma, P.; Schmid, M.; Meyer, T. F. ADP Heptose, a Novel Pathogen-Associated Molecular Pattern Identified in Helicobacter Pylori. *The FASEB Journal* **2019**, *33* (8), 9087–9099. https://doi.org/https://doi.org/10.1096/fj.201802555R.

(42) Liang, L.; Wade Wei, T.-Y.; Wu, P.-Y.; Herrebout, W.; Tsai, M.-D.; Vincent, S. P. Nonhydrolyzable Heptose Bis- and Monophosphate Analogues Modulate Pro-Inflammatory TIFA-NF-KB Signaling. *ChemBioChem* **2020**, *21* (20), 2982–2990. https://doi.org/https://doi.org/10.1002/cbic.202000319.

(43) Fantoni, N. Z.; El-Sagheer, A. H.; Brown, T. A Hitchhiker's Guide to Click-Chemistry with Nucleic Acids. *Chem Rev* **2021**, *121* (12), 7122–7154. https://doi.org/10.1021/acs.chemrev.0c00928.

(44) Brown, G. B.; Du Vigneaud, V. The Effect of Certain Reagents on the Activity of Biotin. **1941**.

(45) Mirkin, C. A.; Letsinger, R. L.; Mucic, R. C.; Storhoff, J. J. A DNA-Based Method for Rationally Assembling Nanoparticles into Macroscopic Materials. *Nature* **1996**, *382* (6592), 607–609. https://doi.org/10.1038/382607a0.

(46) Cutler, J. I.; Auyeung, E.; Mirkin, C. A. Spherical Nucleic Acids. *J Am Chem Soc* **2012**, *134* (3), 1376–1391. https://doi.org/10.1021/ja209351u.

(47) Vasher, M. K.; Yamankurt, G.; Mirkin, C. A. Hairpin-like SiRNA-Based Spherical Nucleic Acids. *J Am Chem Soc* **2022**, *144* (7), 3174–3181. https://doi.org/10.1021/jacs.1c12750.

(48) Kusmierz, C. D.; Bujold, K. E.; Callmann, C. E.; Mirkin, C. A. Defining the Design Parameters for in Vivo Enzyme Delivery Through Protein Spherical Nucleic Acids. *ACS Cent Sci* **2020**, *6* (5), 815–822. https://doi.org/10.1021/acscentsci.0c00313.

(49) Teplensky, M. H.; Evangelopoulos, M.; Dittmar, J. W.; Forsyth, C. M.; Sinegra, A. J.; Wang, S.; Mirkin, C. A. Multi-Antigen Spherical Nucleic Acid Cancer Vaccines. *Nat Biomed Eng* **2023**, *7* (7), 911–927. https://doi.org/10.1038/s41551-022-01000-2.

(50) Yang, J.; Stolee, J. A.; Jiang, H.; Xiao, L.; Kiesman, W. F.; Antia, F. D.; Fillon, Y. A.; Ng, A.; Shi, X. Solid-Phase Synthesis of Phosphorothioate Oligonucleotides Using Sulfurization Byproducts for in Situ Capping. *J Org Chem* **2018**, *83* (19), 11577–11585. https://doi.org/10.1021/acs.joc.8b01553.

(51) Moumné, L.; Marie, A.-C.; Crouvezier, N. Oligonucleotide Therapeutics: From Discovery and Development to Patentability. *Pharmaceutics* **2022**, *14* (2). https://doi.org/10.3390/pharmaceutics14020260.

(52) Bujold, K. E.; Hsu, J. C. C.; Sleiman, H. F. Optimized DNA "Nanosuitcases" for Encapsulation and Conditional Release of SiRNA. *J Am Chem Soc* **2016**, *138* (42), 14030–14038. https://doi.org/10.1021/jacs.6b08369.

(53) Cutler, J. I.; Zhang, K.; Zheng, D.; Auyeung, E.; Prigodich, A. E.; Mirkin, C. A. Polyvalent Nucleic Acid Nanostructures. *J Am Chem Soc* **2011**, *133* (24), 9254–9257. https://doi.org/10.1021/ja203375n.

(54) Rennick, J. J.; Johnston, A. P. R.; Parton, R. G. Key Principles and Methods for Studying the Endocytosis of Biological and Nanoparticle Therapeutics. *Nat Nanotechnol* **2021**, *16* (3), 266–276. https://doi.org/10.1038/s41565-021-00858-8.

(55) Choi, C. H. J.; Hao, L.; Narayan, S. P.; Auyeung, E.; Mirkin, C. A. Mechanism for the Endocytosis of Spherical Nucleic Acid Nanoparticle Conjugates. *Proc Natl Acad Sci U S A* **2013**, *110* (19), 7625–7630. https://doi.org/10.1073/pnas.1305804110.

(56) Steckel, A.; Schlosser, G. An Organic Chemist's Guide to Electrospray Mass Spectrometric Structure Elucidation. *Molecules*. 2019. https://doi.org/10.3390/molecules24030611.

(57) Pavia, D. L.; Lampman, G. M.; Kriz, G. S.; Vyvyan, J. A. *Introduction to Spectroscopy*; Cengage Learning, 2008.

(58) Lopez-Gomollon, S.; Nicolas, F. E. Purification of DNA Oligos by Denaturing Polyacrylamide Gel Electrophoresis (PAGE). *Methods Enzymol* **2013**, *529*, 65–83. https://doi.org/10.1016/B978-0-12-418687-3.00006-9.

(59) Gao, X.; Tan, B.-H.; Sugrue, R. J.; Tang, K. MALDI Mass Spectrometry for Nucleic Acid Analysis BT - Applications of MALDI-TOF Spectroscopy; Cai, Z., Liu, S., Eds.; Springer Berlin Heidelberg: Berlin, Heidelberg, 2013; pp 55–77. https://doi.org/10.1007/128_2012_366.

(60) Sharin, M. D.; Floro, G. M.; Clark, K. D. Advances in Nucleic Acid Sample Preparation for Electrospray Ionization and Matrix-Assisted Laser Desorption Ionization Mass Spectrometry. *Int J Mass Spectrom* **2023**, *494*, 117138. https://doi.org/https://doi.org/10.1016/j.ijms.2023.117138.

(61) Cui, Z.; Theruvathu, J. A.; Farrel, A.; Burdzy, A.; Sowers, L. C. Characterization of Synthetic Oligonucleotides Containing Biologically Important Modified Bases by Matrix-Assisted Laser Desorption/Ionization Time-of-Flight Mass Spectrometry. *Anal Biochem* **2008**, *379* (2), 196–207. https://doi.org/10.1016/J.AB.2008.04.031.

(62) Hossain, M.; Limbach, P. A. A Comparison of MALDI Matrices. In *Electrospray and MALDI Mass Spectrometry*; 2010; pp 215–244. https://doi.org/https://doi.org/10.1002/9780470588901.ch7.

(63) Zemski Berry, K. A.; Hankin, J. A.; Barkley, R. M.; Spraggins, J. M.; Caprioli, R. M.; Murphy, R. C. MALDI Imaging of Lipid Biochemistry in Tissues by Mass Spectrometry. *Chem Rev* **2011**, *111* (10), 6491–6512. https://doi.org/10.1021/cr200280p.

(64) Güzlek, H.; Graziani, A.; Kosma, P. A Short Synthesis of D-Glycero-d-Manno-Heptose 7-Phosphate. *Carbohydr Res* **2005**, *340* (18), 2808–2811. https://doi.org/https://doi.org/10.1016/j.carres.2005.10.003.

(65) Laue, S.; Haverkamp, V.; Mleczko, L. Experience with Scale-Up of Low-Temperature Organometallic Reactions in Continuous Flow. *Org Process Res Dev* **2016**, *20* (2), 480–486. https://doi.org/https://doi.org/10.1021/acs.oprd.5b00183.

(66) Taylor, C. J.; Pomberger, A.; Felton, K. C.; Grainger, R.; Barecka, M.; Chamberlain, T. W.; Bourne, R. A.; Johnson, C. N.; Lapkin, A. A. A Brief Introduction to Chemical Reaction Optimization. *Chem Rev* **2023**, *123* (6), 3089–3126. https://doi.org/10.1021/acs.chemrev.2c00798.

(67) Brimacombe, J. S.; Mengech, A. S.; Tucker, L. C. N. Synthesis of Derivatives of Methyl 2,6-Dideoxy-4-O-Methyl-α-D-Ribo-Hexopyranoside: On the Structure of Variose. *J Chem Soc Perkin 1* **1977**, No. 6, 643–645. https://doi.org/10.1039/P19770000643.

(68) Vlahakis, E.; Halikias, G. Temperature and Concentration Control of Exothermic Chemical Processes in Continuous Stirred Tank Reactors. *Transactions of the Institute of Measurement and Control* **2019**, *41* (15), 4274–4284. https://doi.org/10.1177/0142331219855591.

(69) Bernard, P.; Stelmachowski, P.; Broś, P.; Makowski, W.; Kotarba, A. Demonstration of the Influence of Specific Surface Area on Reaction Rate in Heterogeneous Catalysis. *J Chem Educ* **2021**, *98* (3), 935–940. https://doi.org/10.1021/acs.jchemed.0c01101.

(70) Huang, M.; Xu, X.; Qiu, H.; Li, N. Analytical Characterization of DNA and RNA Oligonucleotides by Hydrophilic Interaction Liquid Chromatography-Tandem Mass Spectrometry. *J Chromatogr A* **2021**, *1648*, 462184. https://doi.org/10.1016/J.CHROMA.2021.462184.

(71) Broadpharm. *DBCO azide ligation protocol*. https://broadpharm.com/protocol_files/dbco_azide_click_chemistry (accessed 2022-01-17).

(72) AlphaThera. *Oyo-Link® DBCO*. https://alphathera.com/product/click-chemistry-chemical-conjugations/oyo-link-dbco/ (accessed 2024-06-30).

(73) Hurst, S. J.; Lytton-Jean, A. K. R.; Mirkin, C. A. Maximizing DNA Loading on a Range of Gold Nanoparticle Sizes. *Anal Chem* **2006**, *78* (24), 8313–8318. https://doi.org/10.1021/ac0613582.

(74) Callmann, C. E.; Vasher, M. K.; Das, A.; Kusmierz, C. D.; Mirkin, C. A. In Vivo Behavior of Ultrasmall Spherical Nucleic Acids. *Small* **2023**, *19* (24), 2300097. https://doi.org/https://doi.org/10.1002/smll.202300097.

(75) Hay, D. W. P.; Sarau, H. M. Interleukin-8 Receptor Antagonists in Pulmonary Diseases. *Curr Opin Pharmacol* **2001**, *1* (3), 242–247. https://doi.org/10.1016/S1471-4892(01)00043-1.

(76) D., M. M.; Michael, K.; Nuttee, S.; Saki, S.; Roshni, M.; Ruth, C.; Gregory, B.; Sung, A. D.; A., Z. J. HIV Latency in the Humanized BLT Mouse. *J Virol* **2012**, *86* (1), 339–347. https://doi.org/10.1128/jvi.06366-11.

(77) Summer, H.; Grämer, R.; Dröge, P. Denaturing Urea Polyacrylamide Gel Electrophoresis (Urea PAGE). *JoVE* **2009**, No. 32, e1485. https://doi.org/doi:10.3791/1485.

(78) Ellington, A.; Pollard Jr., J. D. Introduction to the Synthesis and Purification of Oligonucleotides. *Curr Protoc Nucleic Acid Chem* **2000**, *00* (1), A.3C.1-A.3C.22. https://doi.org/https://doi.org/10.1002/0471142700.nca03cs00.